

A posteriori estimator for the adaptive solution of a quasi-static fracture phase-field model with irreversibility constraints

Mirjam Walloth and Winnifried Wollner

Fachbereich Mathematik, TU Darmstadt

Dolivostraße 15, 64293 Darmstadt

walloth@mathematik.tu-darmstadt.de, wollner@mathematik.tu-darmstadt.de

Friday 18th June, 2021

Abstract

Within this article, we develop a residual type a posteriori error estimator for a time discrete quasi-static phase-field fracture model. Particular emphasize is given to the robustness of the error estimator for the variational inequality governing the phase-field evolution with respect to the phase-field regularization parameter ϵ . The article concludes with numerical examples highlighting the performance of the proposed a posteriori error estimators on three standard test cases; the single edge notched tension and shear test as well as the L-shaped panel test.

Key words. residual-type a posteriori error estimator, Galerkin functional, phase-field fracture, robust a posteriori error estimation

1 Introduction

Modeling of fracture propagation by variational models has a long history. [12] provided a variational formulation of Griffith's model for brittle fracture [14]. See also [7] for a summary. More recently, such phase-field models have increased in complexity incorporating different phenomena, see, e.g., [1, 6, 20, 21, 24] and higher order methods have been proposed, e.g., [5].

Since the interface, where a transition between the broken and unbroken material occurs, is often very narrow adaptive finite element methods have been proposed for the solution of such problems. [8] started by showing that an alternating refinement procedure according to a posteriori error estimators for the elastic material and the phase-field equation in each time step gives rise to a convergent algorithm. This analysis was extended to more general energy functionals in [9]. Improvements towards anisotropic refinements were proposed in [3], all these contributions dealt with the irreversibility condition by fixing the phase-field to 0, i.e., fracture, once a tolerance value had been reached by the phase-field variable. Thereby avoiding a variational inequality for the description of the time-discrete fracture. More heuristic methods, such as a

predictor-corrector scheme based on refinement near the computed fracture [17] or dual-weighted residual error estimates [33] have also been proposed.

Within this article, we will analyze the residual based error estimator proposed in [19] for the a posteriori error estimation within a phase-field fracture model. In contrast to prior work the analysis will treat the irreversibility condition of the phase-field by a variational inequality. Due to the modeling and time discretization this variational inequality is a singularly perturbed obstacle problem and consequently we will show that our estimates are robust [26] with respect to the singular perturbation. Moreover, we will sketch how stress-splitting approaches [20] can be incorporated into the error estimates.

Various methods for a posteriori error estimation of the obstacle problem can be found in the literature, see, e.g., [4, 10, 15, 25, 32, 35]. Here we focus on the approach by [25] utilizing a suitable Galerkin functional and a useful definition of the discrete constraining forces.

The rest of the paper is structured as follows. In Section 2, we will introduce the time-discrete phase-field fracture model under consideration and briefly state its discretization. In Section 3, we introduce some suitable auxiliary problems utilized to decouple the discretization error for the elasticity equation and the phase-field inequality. We continue by defining a discrete counterpart of the constraining force and state the error estimator for the phase-field variable and the Lagrange multiplier for the obstacle. In Section 4, we show the robust reliability of the proposed estimator. This is complemented by the efficiency in Section 5, indeed efficiency is not always robust. It will become robust once the semi-contact zone, near the fracture, is sufficiently resolved. For completeness, in Section 6, we state a standard residual estimator for the elasticity equation in each time step. The paper concludes with numerical examples in Section 7. Here we demonstrate the robustness of the proposed error estimators on three standard test cases, the single edge notched shear and tension tests as well as an L-shaped panel test.

2 A quasi-static fracture phase-field model

Let $\Omega \subset \mathbb{R}^2$ be a polygonal domain of a linear elastic body in which a lower dimensional fracture \mathfrak{C} may exist and propagate. Let $I = (0, T)$ be the time interval. The displacements are given by the function $\mathbf{u} : \Omega \times I \rightarrow \mathbb{R}^2$. Based on the phase-field approach the fracture is approximated by the phase-field variable $\varphi : \Omega \times I \rightarrow [0, 1]$ where $\varphi = 1$ characterizes the unbroken material and $\varphi = 0$ the broken material. The intermediate values constitute a smooth transition zone dependent on a small regularization parameter ϵ . The physics of the underlying problem ask to enforce that the fracture cannot heal. This condition is called irreversibility condition.

The boundary $\Gamma = \partial\Omega$ is subdivided in Dirichlet Γ^D and Neumann boundary Γ^N where we enforce Dirichlet and Neumann boundary values for the displacements \mathbf{u} . For the phase-field variable, we have Neumann values $\nabla\varphi \cdot \mathbf{n} = 0$ on the whole boundary where \mathbf{n} is the unit outward normal to the boundary.

We denote the critical energy release rate by G_c . A degradation function is defined as $g(\varphi) := (1 - \kappa)\varphi^2 + \kappa$ where κ is a small regularization parameter.

The stress tensor $\boldsymbol{\sigma}(\mathbf{u})$ is given by

$$\boldsymbol{\sigma}(\mathbf{u}) := 2\mu \mathbf{E}_{\text{lin}}(\mathbf{u}) + \lambda \text{tr}(\mathbf{E}_{\text{lin}}(\mathbf{u})) \mathbf{id}.$$

Here, λ and μ are the Lamé constants, $\mathbf{E}_{\text{lin}}(\mathbf{u})$ is the linearized strain tensor:

$$\mathbf{E}_{\text{lin}}(\mathbf{u}) := \frac{1}{2}(\nabla \mathbf{u} + \nabla \mathbf{u}^T),$$

and \mathbf{id} denotes the two-dimensional identity matrix. Often the relation between $\boldsymbol{\sigma}$ and \mathbf{E}_{lin} is given by means of Hooke's tensor, i.e.

$$\sigma_{ij}(\mathbf{u}) = C_{ijml}(\mathbf{E}_{\text{lin}}(\mathbf{u}))_{ml}$$

where C_{ijml} are the components of Hooke's tensor which is symmetric, elliptic and bounded.

We consider a time discrete formulation on a fixed subdivision $0 = t_0 < t_1 < \dots < t_N = T$ of the interval I . We define approximations $(\mathbf{u}^n, \varphi^n) \approx (\mathbf{u}(t_n), \varphi(t_n))$ and enforce a so-called discrete irreversibility condition given by $\varphi^n \leq \varphi^{n-1}$ for all $n = 1, \dots, N$. The discrete irreversibility condition is an approximation of the condition that the fracture cannot heal.

In each time step, we seek the displacement variable in $\mathcal{H}_D^n := \{\mathbf{v} \in \mathbf{H}^1(\Omega) \mid \text{tr}|_{\Gamma_D}(\mathbf{v}) = \mathbf{u}_D(t^n) \text{ a.e. on } \Gamma_D\}$. Further, we need the test space $\mathcal{H}_0 := \{\mathbf{w} \in \mathbf{H}^1(\Omega) \mid \text{tr}|_{\Gamma_D}(\mathbf{w}) = \mathbf{0} \text{ a.e. on } \Gamma_D\}$. To give the weak formulation in each time step n , we define the feasible set $\mathcal{K}(\varphi^{n-1}) := \{\psi \in H^1(\Omega) \mid \psi \leq \varphi^{n-1} \leq 1\}$ for the phase-field variable. We denote the L^2 -scalar product by $\langle \cdot, \cdot \rangle$ and dual pairings by $\langle \cdot, \cdot \rangle_{-1,1}$.

Thus, the weak problem formulation in each time step n is given by

Problem 1 (Weak formulation in each time step). *Find $(\mathbf{u}^n, \varphi^n) \in \mathcal{H}_D^n \times \mathcal{K}(\varphi^{n-1})$ such that*

$$\begin{aligned} \langle g(\varphi^{n-1}) \boldsymbol{\sigma}(\mathbf{u}^n), \mathbf{E}_{\text{lin}}(\mathbf{w}) \rangle &= 0 \quad \forall \mathbf{w} \in \mathcal{H}_0 \\ \langle (1 - \kappa) \varphi^n \boldsymbol{\sigma}(\mathbf{u}^n) : \mathbf{E}_{\text{lin}}(\mathbf{u}^n), \psi - \varphi^n \rangle & \\ - \frac{G_c}{\epsilon} \langle 1 - \varphi^n, \psi - \varphi^n \rangle + \epsilon G_c \langle \nabla \varphi^n, \nabla(\psi - \varphi^n) \rangle &\geq 0 \quad \forall \psi \in \mathcal{K}(\varphi^{n-1}) \end{aligned} \quad (1)$$

In Miehe et al. [21] a stress splitting into a crack driving and a non crack driving part has been proposed for fracture phase-field models. The linearized strain tensor is decomposed into its tensile and compressive parts, i.e., $\mathbf{E}_{\text{lin}} := \mathbf{E}_{\text{lin}}^+ + \mathbf{E}_{\text{lin}}^-$ with

$$\mathbf{E}_{\text{lin}}^+ := \mathbf{Q} \mathbf{D}^+ \mathbf{Q}^T$$

where \mathbf{Q} is the matrix of eigenvectors, of \mathbf{E}_{lin} , and \mathbf{D} the matrix with the corresponding eigenvalues on the diagonal. Further, $(\cdot)^+$ denotes the positive part, i.e., on the diagonal of \mathbf{D}^+ are either the positive eigenvalues or zeros. We use the stress splitting of [21] which is given by

$$\begin{aligned} \boldsymbol{\sigma}^+(\mathbf{u}) &:= 2\mu \mathbf{E}_{\text{lin}}^+(\mathbf{u}) + \lambda \max\{0, \text{tr}(\mathbf{E}_{\text{lin}}(\mathbf{u}))\} \mathbf{id}, \\ \boldsymbol{\sigma}^-(\mathbf{u}) &:= 2\mu \mathbf{E}_{\text{lin}}^-(\mathbf{u}) + \lambda \min\{0, \text{tr}(\mathbf{E}_{\text{lin}}(\mathbf{u}))\} \mathbf{id} \end{aligned}$$

where $\boldsymbol{\sigma}^+$ is the crack driving part of the stress. With these definitions and notations the time discrete weak formulation of the quasi-static fracture phase-field model according to [21] reads as follows

Problem 2 (Weak formulation in each time step with Miehe stress splitting).
Find $(\mathbf{u}^n, \varphi^n) \in \mathcal{H}_D^n \times \mathcal{K}(\varphi^{n-1})$ such that

$$\begin{aligned} \langle g(\varphi^{n-1})\boldsymbol{\sigma}^+(\mathbf{u}^n) + \boldsymbol{\sigma}^-(\mathbf{u}^n), \mathbf{E}_{\text{lin}}(\mathbf{w}) \rangle &= 0 \quad \forall \mathbf{w} \in \mathcal{H}_0 \\ \langle (1 - \kappa)\varphi^n \boldsymbol{\sigma}^+(\mathbf{u}^n) : \mathbf{E}_{\text{lin}}(\mathbf{u}^n), \psi - \varphi^n \rangle & \\ -\frac{G_c}{\epsilon} \langle 1 - \varphi^n, \psi - \varphi^n \rangle + \epsilon G_c \langle \nabla \varphi^n, \nabla(\psi - \varphi^n) \rangle &\geq 0 \quad \forall \psi \in \mathcal{K}(\varphi^{n-1}) \end{aligned} \quad (2)$$

2.1 Discrete formulation

In the discrete setting, at each time step $n = 1, \dots, N$, we decompose the polygonal domain Ω by a (family of) meshes \mathfrak{M}^n consisting of shape regular parallelograms or triangles $\boldsymbol{\epsilon}$, such that all meshes share a common coarse mesh. To allow for local refinement, in particular of rectangular elements, we allow for one hanging node per edge at which degrees of freedom will be eliminated to assert conformity of the discrete spaces. Further, we assume that the boundary of the domain is resolved by the chosen meshes.

To each mesh, we associate the mesh size function h^n , i.e., $h_{\boldsymbol{\epsilon}}^n = h^n|_{\boldsymbol{\epsilon}} = \text{diam } \boldsymbol{\epsilon}$ for any element $\boldsymbol{\epsilon} \in \mathfrak{M}^n$. The set of nodes p is given by \mathfrak{N} and we distinguish between the set \mathfrak{N}^Γ of nodes at the boundary and the set of interior nodes \mathfrak{N}^I . Further, for a point $p \in \mathfrak{N}$, we define a patch ω_p as the interior of the union of all elements sharing the node p . We call the union of all sides in the interior of ω_p , not including the boundary of ω_p , skeleton and denote it by γ_p^I . For boundary nodes, we denote the intersections between Γ and $\partial\omega_p$ by $\gamma_p^\Gamma := \Gamma \cap \partial\omega_p$. Further, we will make use of $\omega_{\mathfrak{s}}$ which is the union of all elements sharing a side \mathfrak{s} . Later on, we need the definition of the jump term $[\nabla\psi_h] := \nabla|_{\boldsymbol{\epsilon}}\psi_h \cdot \mathbf{n}_{\boldsymbol{\epsilon}} - \nabla|_{\tilde{\boldsymbol{\epsilon}}}\psi_h \cdot \mathbf{n}_{\tilde{\boldsymbol{\epsilon}}}$ where $\boldsymbol{\epsilon}, \tilde{\boldsymbol{\epsilon}}$ are neighboring elements and $\mathbf{n}_{\boldsymbol{\epsilon}}$ is the unit outward normal on the common side of the two elements. For the discretization, we consider linear finite elements on triangles and bilinear finite elements on parallelograms. We abbreviate

$$\mathbb{S}_1(\boldsymbol{\epsilon}) := \begin{cases} \mathbb{P}_1(\boldsymbol{\epsilon}), & \text{if } \boldsymbol{\epsilon} \text{ is a triangle,} \\ \mathbb{Q}_1(\boldsymbol{\epsilon}), & \text{if } \boldsymbol{\epsilon} \text{ is a parallelogram.} \end{cases}$$

We define the space of continuous (bi-)linear finite elements by

$$\mathcal{H}_{\mathfrak{m}} := \{\zeta_{\mathfrak{m}} \in \mathcal{C}^0(\bar{\Omega}) \mid \forall \boldsymbol{\epsilon} \in \mathfrak{M}, \zeta_{\mathfrak{m}}|_{\boldsymbol{\epsilon}} \in \mathbb{S}_1(\boldsymbol{\epsilon})\}.$$

The nodal basis functions of the finite element spaces are denoted by ϕ_p . Hence, a finite element function has the representation

$$\zeta_{\mathfrak{m}} = \sum_{p \in \mathfrak{N}} \zeta_{\mathfrak{m}}(p) \phi_p.$$

We assume the Dirichlet data $\mathbf{u}_D(t^n) \in \mathcal{C}^0$ to be continuous and piecewise linear on the coarsest meshes. Thus, we seek the discrete displacements in the subset

$$\mathcal{H}_{\mathfrak{m},D}^n := \{\mathbf{v}_{\mathfrak{m}} \in \mathcal{C}^0(\bar{\Omega}) \mid \forall \boldsymbol{\epsilon} \in \mathfrak{M}^n, \mathbf{v}_{\mathfrak{m}}|_{\boldsymbol{\epsilon}} \in \mathbb{S}_1(\boldsymbol{\epsilon}) \text{ and } \mathbf{v}_{\mathfrak{m}} = \mathbf{u}_D(t^n) \text{ on } \Gamma^D\}.$$

The corresponding discrete test space is given by

$$\mathcal{H}_{\mathfrak{m},0}^n := \{\mathbf{v}_{\mathfrak{m}} \in \mathcal{C}^0(\bar{\Omega}) \mid \forall \boldsymbol{\epsilon} \in \mathfrak{M}^n, \mathbf{v}_{\mathfrak{m}}|_{\boldsymbol{\epsilon}} \in \mathbb{S}_1(\boldsymbol{\epsilon}) \text{ and } \mathbf{v}_{\mathfrak{m}} = \mathbf{0} \text{ on } \Gamma^D\}.$$

For the discrete phase-field variable the discrete feasible set is given by

$$\mathcal{K}_m^n := \{\psi_m \in \mathcal{H}_m \mid \psi_m(p) \leq I_m^n(\varphi_m^{n-1})(p), \forall p \in \mathfrak{N}\}$$

where I_m^n is the nodal interpolation operator on the mesh \mathfrak{M}^n .

Thus, the discrete formulation of Problem 1 is given by

Problem 3 (Discrete formulation in each time step). *Find $(\mathbf{u}_m^n, \varphi_m^n) \in \mathcal{H}_{m,D}^n \times \mathcal{K}_m^n$ such that*

$$\begin{aligned} \langle g(\varphi_m^{n-1})\boldsymbol{\sigma}(\mathbf{u}_m^n), \mathbf{E}_{\text{lin}}(\mathbf{w}_m) \rangle &= 0 \quad \forall \mathbf{w}_m \in \mathcal{H}_{m,0}^n \\ \langle (1 - \kappa)\varphi_m^n \boldsymbol{\sigma}(\mathbf{u}_m^n) : \mathbf{E}_{\text{lin}}(\mathbf{u}_m^n), \psi_m - \varphi_m^n \rangle & \\ - \frac{G_c}{\epsilon} \langle 1 - \varphi_m^n, \psi_m - \varphi_m^n \rangle + \epsilon G_c \langle \nabla \varphi_m^n, \nabla(\psi_m - \varphi_m^n) \rangle &\geq 0 \quad \forall \psi_m \in \mathcal{K}_m^n \end{aligned} \quad (3)$$

Using the splitting proposed in [21], we get

Problem 4 (Discrete formulation in each time step with Miehe stress splitting). *Find $(\mathbf{u}_m^n, \varphi_m^n) \in \mathcal{H}_{m,D}^n \times \mathcal{K}_m^n$ such that*

$$\begin{aligned} \langle g(\varphi_m^{n-1})\boldsymbol{\sigma}^+(\mathbf{u}_m^n) + \boldsymbol{\sigma}^-(\mathbf{u}_m^n), \mathbf{E}_{\text{lin}}(\mathbf{w}_m) \rangle &= 0 \quad \forall \mathbf{w}_m \in \mathcal{H}_{m,0}^n \\ \langle (1 - \kappa)\varphi_m^n \boldsymbol{\sigma}^+(\mathbf{u}_m^n) : \mathbf{E}_{\text{lin}}(\mathbf{u}_m^n), \psi_m - \varphi_m^n \rangle & \\ - \frac{G_c}{\epsilon} \langle 1 - \varphi_m^n, \psi_m - \varphi_m^n \rangle + \epsilon G_c \langle \nabla \varphi_m^n, \nabla(\psi_m - \varphi_m^n) \rangle &\geq 0 \quad \forall \psi_m \in \mathcal{K}_m^n \end{aligned} \quad (4)$$

3 Residual-type a posteriori estimator for the variational inequality

In this section, we propose a residual-type a posteriori estimator for the adaptive solution of the quasi-static phase-field model (Problems 1 and 3). We comment on how the estimator changes for the problem formulations with the stress splitting (Problem 2 and Problem 4). As the structure remains the same for all time steps, we consider one time step n , only. We drop the now superfluous superscript n for the solution and for other quantities as e.g., $h_\epsilon := h_\epsilon^n$.

The proofs of reliability and efficiency are given in Sections 4 and 5.

3.1 Auxiliary problem formulation

The residual-type a posteriori estimator proposed in this section is derived for the solution of the following variational inequality (Problem 5).

Problem 5. *Let \mathbf{u}_m^n and φ_m^{n-1} be given, then find $\hat{\varphi} \in \mathcal{K}(I_m^n(\varphi_m^{n-1}))$ such that*

$$a_{m,\epsilon}(\hat{\varphi}, \psi - \hat{\varphi}) \geq \left\langle \frac{G_c}{\epsilon}, \psi - \hat{\varphi} \right\rangle \quad \forall \psi \in \mathcal{K}(I_m^n(\varphi_m^{n-1})) \quad (5)$$

where the bilinear form is given by

$$a_{m,\epsilon}(\zeta, \psi) := \left\langle \left(\frac{G_c}{\epsilon} + (1 - \kappa) (\boldsymbol{\sigma}(\mathbf{u}_m^n) : \mathbf{E}_{\text{lin}}(\mathbf{u}_m^n)) \right) \zeta, \psi \right\rangle + G_c \epsilon \langle \nabla \zeta, \nabla \psi \rangle, \quad (6)$$

and $\mathcal{K}(I_m^n(\varphi_m^{n-1})) := \{\psi \in \mathcal{H} \mid \psi \leq I_m^n(\varphi_m^{n-1})\}$.

It exists a distribution $\hat{\Lambda} \in H^{-1}$, called constraining force density, which turns the variational inequality (5) into an equation

$$\langle \hat{\Lambda}, \psi \rangle_{-1,1} := \left\langle \frac{G_c}{\epsilon}, \psi \right\rangle - a_{m,\epsilon}(\hat{\varphi}, \psi) \quad \forall \psi \in H^1.$$

As discrete approximation of Problem 5, we consider the following Problem

Problem 6. Let \mathbf{u}_m^n and φ_m^{n-1} be given, then find $\hat{\varphi}_m \in \mathcal{K}_m^n$ such that

$$a_{m,\epsilon}(\hat{\varphi}_m, \psi_m - \hat{\varphi}_m) \geq \left\langle \frac{G_c}{\epsilon}, \psi_m - \hat{\varphi}_m \right\rangle \quad \forall \psi_m \in \mathcal{K}_m^n \quad (7)$$

We define the corresponding discrete constraining force density $\hat{\Lambda}_m \in \mathcal{H}_m^*$ as

$$\langle \hat{\Lambda}_m, \psi_m \rangle_{-1,1} := \left\langle \frac{G_c}{\epsilon}, \psi_m \right\rangle - a_{m,\epsilon}(\hat{\varphi}_m, \psi_m) \quad \forall \psi_m \in \mathcal{H}_m. \quad (8)$$

We note that the discrete solution $\hat{\varphi}_m$ of (7) equals the discrete solution φ_m^n of Problem 3 in time step n . Further, as the bilinear form $a_{m,\epsilon}(\cdot, \cdot)$ depends on the approximation \mathbf{u}_m^n of \mathbf{u}^n and the constraints depend on the approximation $I_m^n(\varphi_m^{n-1})$ of φ^{n-1} , the solution $\hat{\varphi}$ of (5) is an approximation to the solution φ^n of (1).

3.2 Error measure and quasi-discrete constraining force

The error will be measured in the solution of the variational inequality as well as in the constraining forces as has been proposed in [25] for the obstacle problem. We measure the error of the solution $\hat{\varphi}$ in the energy norm

$$\|\cdot\|_\epsilon := \left\{ G_c \epsilon \|\nabla(\cdot)\|^2 + \left\| \left(\frac{G_c}{\epsilon} + (1 - \kappa)\boldsymbol{\sigma}(\mathbf{u}_m^n) : \mathbf{E}_{\text{lin}}(\mathbf{u}_m^n) \right) (\cdot) \right\|^2 \right\}^{\frac{1}{2}} \quad (9)$$

which corresponds to the bilinear form $a_{m,\epsilon}(\cdot, \cdot)$.

Remark 1. We note that in the case of stress splitting $\boldsymbol{\sigma} : \mathbf{E}_{\text{lin}}$ in (6) and in (9) is replaced by $\boldsymbol{\sigma}^+ : \mathbf{E}_{\text{lin}}$. The resulting bilinear form is positive definite as

$$\begin{aligned} \boldsymbol{\sigma}^+ : \mathbf{E}_{\text{lin}} &= 2\mu \mathbf{E}_{\text{lin}}^+ : \mathbf{E}_{\text{lin}} + \lambda \max\{0, \text{tr}(\mathbf{E}_{\text{lin}})\} \mathbf{id} : \mathbf{E}_{\text{lin}} \\ &= 2\mu (\mathbf{QD}^+ \mathbf{Q}^T) : (\mathbf{QDQ}^T) + \lambda \max\{0, \text{tr}(\mathbf{E}_{\text{lin}})\} \mathbf{id} : \mathbf{E}_{\text{lin}} \\ &= 2\mu \text{tr}(\mathbf{D}^+)^2 + \lambda \max\{0, \text{tr}(\mathbf{E}_{\text{lin}})\}^2 > 0. \end{aligned} \quad (10)$$

Thus, the energy norm is well defined.

The error in the constraining forces is measured in the corresponding dual norm

$$\|\cdot\|_{*,\epsilon} := \frac{\sup_{\psi \in H^1} \langle \cdot, \psi \rangle_{-1,1}}{\|\psi\|_\epsilon}.$$

In order to compare the continuous and discrete constraining forces, we cannot simply take $\hat{\Lambda}_m$ given by definition (8) as it is a functional on the space of discrete functions, only, and not a functional on H^1 . There is no unique definition how

$\hat{\Lambda}_m$ acts on a function in H^1 which is not in \mathcal{H}_m . Thus, we have to define a suitable approximation of $\hat{\Lambda}$ as a functional on H^1 on the basis of the properties of the discrete solution $\hat{\varphi}_m$ and $\hat{\Lambda}_m$. We call it quasi-discrete constraining force and denote it by $\tilde{\Lambda}_m$. In [25] such a functional on H^1 has been proposed by means of lumping $\sum_{p \in \mathfrak{N}^C} s_p \phi_p$, where $s_p = \frac{\langle \hat{\Lambda}_m, \phi_p \rangle_{-1,1}}{\int_{\omega_p} \phi_p} \geq 0$ are the node values of the lumped discrete constraining force. The sign condition follows from the discrete variational inequality. As the lumped discrete constraining force is a discrete function a complementarity condition, i.e., $\hat{\Lambda}_m \cdot (\hat{\varphi}_m - I_m^n(\varphi_m^{n-1})) = 0$, cannot be fulfilled in the so-called semi-contact zone which consists of elements having nodes which are in contact and nodes which are not in contact. It is only valid in so-called full-contact areas where $\hat{\varphi}_m = I_m^n(\varphi_m^{n-1})$ and in non-actual-contact areas where $\hat{\varphi}_m < I_m^n(\varphi_m^{n-1})$.

Especially for the efficiency and the localization of a posteriori error estimation it is very advantageous, if the quasi-discrete constraining force density can be defined differently for the different areas of full- and semi-contact to reflect local properties. Such an approach has been used first for the derivation of an a posteriori error estimator in [11] and applied to obstacle and contact problems in, e.g., [15, 16, 18, 22, 23, 30, 31]. Following this approach, we distinguish between full-contact nodes $p \in \mathfrak{N}^{fC}$ and semi-contact nodes $p \in \mathfrak{N}^{sC}$. Full-contact nodes are those nodes for which the solution is fixed to the obstacle, i.e., $\hat{\varphi}_m^n = I_m^n(\varphi_m^{n-1})$ on ω_p , and the sign condition

$$0 \leq \langle \mathcal{R}_m^{lin}, \psi \rangle_{-1,1,\omega_p} := \left\langle \frac{G_c}{\epsilon}, \psi \right\rangle - a_{m,\epsilon}(\hat{\varphi}_m, \psi) \quad \forall \psi \geq 0 \in \mathcal{H}_0(\omega_p)$$

is fulfilled. The latter condition means that the solution is locally not improvable, see the explanation in [22]. Semi-contact nodes are those nodes for which $\hat{\varphi}_m^n(p) = I_m^n(\varphi_m^{n-1})(p)$ holds but not the above conditions of full-contact. Based on this classification, we define the quasi-discrete constraining force

$$\langle \tilde{\Lambda}_m, \psi \rangle_{-1,1} := \sum_{p \in \mathfrak{N}^{sC}} \langle \tilde{\Lambda}_m^p, \psi \phi_p \rangle_{-1,1} + \sum_{p \in \mathfrak{N}^{fC}} \langle \tilde{\Lambda}_m^p, \psi \phi_p \rangle_{-1,1}. \quad (11)$$

For the definition of the local contributions, we abbreviate the element residual

$$r(\hat{\varphi}_m) := \frac{G_c}{\epsilon} + G_c \epsilon \Delta \hat{\varphi}_m - \frac{G_c}{\epsilon} \hat{\varphi}_m - (1 - \kappa)(\boldsymbol{\sigma}(\mathbf{u}_m^n) : \mathbf{E}_{lin}(\mathbf{u}_m^n)) \hat{\varphi}_m. \quad (12)$$

For semi-contact nodes we consider the following local contribution in (11)

$$\begin{aligned} \langle \tilde{\Lambda}_m^p, \psi \phi_p \rangle_{-1,1} &:= \langle \hat{\Lambda}_m, \phi_p \rangle_{-1,1} c_p(\psi) \\ &= \int_{\gamma_p^I} G_c \epsilon [\nabla \hat{\varphi}_m] c_p(\psi) \phi_p - \int_{\gamma_p^\Gamma} (G_c \epsilon \nabla \hat{\varphi}_m \cdot \mathbf{n}_\epsilon) c_p(\psi) \phi_p + \int_{\omega_p} r(\hat{\varphi}_m) c_p(\psi) \phi_p \end{aligned}$$

with $c_p(\psi) = \frac{\int_{\tilde{\omega}_p} \psi \phi_p}{\int_{\tilde{\omega}_p} \phi_p}$, where $\tilde{\omega}_p$ is the patch around p with respect to a three times uniformly red-refined mesh.

For full-contact nodes we define the following local contribution in (11)

$$\begin{aligned} \langle \tilde{\Lambda}_m, \psi \phi_p \rangle_{-1,1} &:= \langle \mathcal{R}_m^{lin}, \psi \phi_p \rangle_{-1,1} \\ &:= \int_{\gamma_p^I} G_c \epsilon [\nabla \hat{\varphi}_m] \psi \phi_p - \int_{\gamma_p^I} (G_c \epsilon \nabla \hat{\varphi}_m \cdot \mathbf{n}_\epsilon) \psi \phi_p + \int_{\omega_p} r(\hat{\varphi}_m) \psi \phi_p. \end{aligned}$$

With these definitions, we define the error measure

$$\|\hat{\varphi} - \hat{\varphi}_m\|_\epsilon + \|\hat{\Lambda} - \tilde{\Lambda}_m\|_{*,\epsilon}. \quad (13)$$

3.3 Error estimator

In order to state the error estimator for the error measure (13), we define for each node p

$$\alpha_p := \min_{x \in \omega_p} \left\{ \frac{G_c}{\epsilon} + (1 - \kappa)(\boldsymbol{\sigma}(\mathbf{u}_m^n) : \mathbf{E}_{lin}(\mathbf{u}_m^n)) \right\} \quad (14)$$

and $h_p := \text{diam}(\omega_p)$. We note that for linear finite elements on triangles the quantity $(\frac{G_c}{\epsilon} + (1 - \kappa)(\boldsymbol{\sigma}^+(\mathbf{u}_m^n) : \mathbf{E}_{lin}(\mathbf{u}_m^n)))$ is constant on each element. The error estimator

$$\eta^\varphi := \sum_{k=1}^4 \eta_k^\varphi \quad (15)$$

for which we prove reliability and efficiency in Sections 4 and 5 consists of the following local contributions

$$\begin{aligned} (\eta_1^\varphi)^2 &:= \sum_{p \in \mathfrak{N} \setminus \mathfrak{N}^I \cup \mathfrak{N}^C} (\eta_{1,p}^\varphi)^2, \quad \eta_{1,p}^\varphi := \min \left\{ \frac{h_p}{\sqrt{G_c \epsilon}}, \alpha_p^{-\frac{1}{2}} \right\} \|r(\hat{\varphi}_m)\|_{\omega_p} \\ (\eta_2^\varphi)^2 &:= \sum_{p \in \mathfrak{N} \setminus \mathfrak{N}^I \cup \mathfrak{N}^C} (\eta_{2,p}^\varphi)^2, \quad \eta_{2,p}^\varphi := \min \left\{ \frac{h_p}{\sqrt{G_c \epsilon}}, \alpha_p^{-\frac{1}{2}} \right\}^{\frac{1}{2}} (G_c \epsilon)^{-\frac{1}{4}} \|G_c \epsilon [\nabla \hat{\varphi}_m]\|_{\gamma_p^I} \\ (\eta_3^\varphi)^2 &:= \sum_{p \in \mathfrak{N} \setminus \mathfrak{N}^I \cup \mathfrak{N}^C} (\eta_{3,p}^\varphi)^2, \quad \eta_{3,p}^\varphi := \min \left\{ \frac{h_p}{\sqrt{G_c \epsilon}}, \alpha_p^{-\frac{1}{2}} \right\}^{\frac{1}{2}} (G_c \epsilon)^{-\frac{1}{4}} \|G_c \epsilon \nabla \hat{\varphi}_m \cdot \mathbf{n}_\epsilon\|_{\gamma_p^I} \\ (\eta_4^\varphi)^2 &:= \sum_{p \in \mathfrak{N}^{sC}} (\eta_{4,p}^\varphi)^2, \quad \eta_{4,p}^\varphi := \left(s_p \int_{\tilde{\omega}_p} (I_m^n(\varphi_m^{n-1}) - \hat{\varphi}_m) \phi_p \right)^{\frac{1}{2}} \end{aligned}$$

with $s_p := \frac{\langle \hat{\Lambda}_m, \phi_p \rangle_{-1,1}}{\int_{\omega_p} \phi_p}$. We emphasize that the estimator contributions related to the constraints are localized to the area of semi-contact. In the absence of any contact, we have $\eta_{k,p}^\varphi = 0$ for $k = 4$ such that η^φ reduces to a robust residual estimator, see, e.g., [26] for the prototype of a singularly perturbed reaction-diffusion equation.

Remark 2. If stress splitting of $\boldsymbol{\sigma}$ is used, the definitions of $r(\hat{\varphi}_m)$ in (12) and α_p in (14) need to consider $\boldsymbol{\sigma}^+$, which thus enters into the error estimator.

In Section 4, we prove that η^φ constitutes a robust upper bound where robust means that the constant in the bound does not depend on ϵ such that the validity of the estimator holds for arbitrary choices of ϵ .

Theorem 1. Reliability of the error estimator

The error estimator η^φ provides a robust upper bound of the error measure (13):

$$\|\hat{\varphi} - \hat{\varphi}_m\|_\epsilon + \|\hat{\Lambda} - \tilde{\Lambda}_m\|_{*,\epsilon} \lesssim \eta^\varphi.$$

In order to formulate the local lower bounds we denote by $\bar{r}(\hat{\varphi}_m)$ a piecewise linear approximations of $r(\hat{\varphi}_m)$ and we abbreviate $\text{osc}_p(r) := \min\{\frac{h_p}{\sqrt{G_c\epsilon}}, \alpha_p^{-\frac{1}{2}}\} \|\bar{r}(\hat{\varphi}_m) - r(\hat{\varphi}_m)\|_{\omega_p}$. In Section 5, we derive the local lower bounds which are summarized in the following Theorems.

Theorem 2. Local lower bounds by $\eta_{1,p}^\varphi, \eta_{2,p}^\varphi, \eta_{3,p}^\varphi$

The error estimator contributions $\eta_{k,p}^\varphi$, $k = 1, 2, 3$ constitute the following robust local lower bounds

$$\eta_{k,p}^\varphi \lesssim \|\hat{\varphi} - \hat{\varphi}_m\|_{\epsilon,\omega_p} + \|\hat{\Lambda} - \tilde{\Lambda}_m\|_{*,\epsilon,\omega_p} + \text{osc}_p(r).$$

To formulate the local lower bound by $\eta_{4,p}^\varphi$ we make use of the definition $\overline{\nabla|_\epsilon v_m} := \nabla|_\epsilon v_m(\zeta_\epsilon)$ as a piecewise constant approximation of $\nabla|_\epsilon v_m$ for $v_m \in \mathcal{H}_m$, where $\zeta_\epsilon \in \epsilon$ is a suitably chosen point that will be defined in the proof of Theorem 3.

Theorem 3. Local lower bound by $\eta_{4,p}^\varphi$

For nodes $p \in \mathfrak{N}^{sC}$ with $\frac{h_p}{\sqrt{G_c\epsilon}} \leq \alpha_p^{-\frac{1}{2}}$ we have the robust local lower bound

$$\begin{aligned} \eta_{4,p}^\varphi \lesssim & \|\hat{\varphi} - \hat{\varphi}_m\|_{\epsilon,\omega_p} + \|\hat{\Lambda} - \tilde{\Lambda}_m\|_{*,\epsilon,\omega_p} + \text{osc}_p(r) \\ & + \min\left\{\frac{h_p}{\sqrt{G_c\epsilon}}, \alpha_p^{-\frac{1}{2}}\right\}^{\frac{1}{2}} (G_c\epsilon)^{-\frac{1}{4}} \|G_c\epsilon \overline{[\nabla(I_m^n(\varphi_m^{n-1}) - \hat{\varphi}_m)]}\|_{\gamma_p^I} \end{aligned} \quad (16)$$

Otherwise, for nodes $p \in \mathfrak{N}^{sC}$ with $\alpha_p^{-\frac{1}{2}} < \frac{h_p}{\sqrt{G_c\epsilon}}$ we have the local lower bound

$$\begin{aligned} \eta_{4,p}^\varphi \lesssim & \|\hat{\varphi} - \hat{\varphi}_m\|_{\epsilon,\omega_p} + \|\hat{\Lambda} - \tilde{\Lambda}_m\|_{*,\epsilon,\omega_p} + \text{osc}_p(r) \\ & + \max\{\alpha_p(G_c\epsilon)^{-2}, \alpha_p^{\frac{1}{2}}(G_c\epsilon)^{-\frac{3}{2}}\} \|G_c\epsilon \overline{[\nabla(I_m^n(\varphi_m^{n-1}) - \hat{\varphi}_m)]}\|_{\gamma_p^I}^2. \end{aligned} \quad (17)$$

Remark 3. We note that the additional term in the bound (16) only occurs for $p \in \mathfrak{N}^{sC}$ and is of the same order as the other estimator contributions. In the application, we expect the semi-contact zone to be well resolved, especially with respect to ϵ meaning $\frac{h_p}{\sqrt{G_c\epsilon}} \leq \alpha_p^{-\frac{1}{2}}$ after a finite number of adaptive refinement steps such that the local lower bound is robust everywhere.

4 Reliability of the estimator

To derive the error estimator, we replace the linear residual which is used in the derivation of a posteriori estimators for linear elliptic equations by a so-called

Galerkin functional which takes into account the errors in both unknowns

$$\begin{aligned}
\langle \mathcal{G}_m, \psi \rangle_{-1,1} &:= a_{m,\epsilon}(\hat{\varphi} - \hat{\varphi}_m, \psi) + \langle \hat{\Lambda} - \tilde{\Lambda}_m, \psi \rangle_{-1,1} \\
&= \left\langle \frac{G_c}{\epsilon}, \psi \right\rangle - a_{m,\epsilon}(\hat{\varphi}_m, \psi) - \langle \tilde{\Lambda}_m, \psi \rangle_{-1,1} \\
&= \sum_{p \in \mathcal{N} \setminus \mathcal{N}^f \cup \mathcal{C}} \left(\int_{\gamma_p^I} G_c \epsilon [\nabla \hat{\varphi}_m](\psi - c_p(\psi)) \phi_p \right. \\
&\quad \left. - \int_{\gamma_p^F} (G_c \epsilon \nabla \hat{\varphi}_m \cdot \mathbf{n}_\epsilon)(\psi - c_p(\psi)) \phi_p + \int_{\omega_p} r(\hat{\varphi}_m)(\psi - c_p(\psi)) \phi_p \right). \tag{18}
\end{aligned}$$

Where the last equality is obtained as usual by utilizing Galerkin-orthogonality and element-wise integration by parts.

The relation between the dual norm of the Galerkin functional $\|\mathcal{G}_m\|_{*,\epsilon}$ and the error measure (13) follows from

$$\|\mathcal{G}_m\|_{*,\epsilon} \lesssim \|\hat{\varphi} - \hat{\varphi}_m\|_\epsilon + \|\hat{\Lambda} - \tilde{\Lambda}_m\|_{*,\epsilon}, \tag{19}$$

and

$$\|\hat{\varphi} - \hat{\varphi}_m\|_\epsilon^2 \leq \|\mathcal{G}_m\|_{*,\epsilon}^2 + 2 \langle \tilde{\Lambda}_m - \hat{\Lambda}, \hat{\varphi} - \hat{\varphi}_m \rangle_{-1,1}, \tag{20}$$

and

$$\|\hat{\Lambda} - \tilde{\Lambda}_m\|_{*,\epsilon}^2 \leq 2 (\|\mathcal{G}_m\|_{*,\epsilon}^2 + \|\hat{\varphi} - \hat{\varphi}_m\|_\epsilon^2), \tag{21}$$

compare [25, Lemma 3.4].

Based on the combination of (20) and (21)

$$\|\hat{\varphi} - \hat{\varphi}_m\|_\epsilon^2 + \|\hat{\Lambda} - \tilde{\Lambda}_m\|_{*,\epsilon}^2 \leq 5 \|\mathcal{G}_m\|_{*,\epsilon}^2 + 6 \langle \tilde{\Lambda}_m - \hat{\Lambda}, \hat{\varphi} - \hat{\varphi}_m \rangle_{-1,1} \tag{22}$$

the reliability of the estimator follows from a computable upper bound of $\|\mathcal{G}_m\|_{*,\epsilon}^2$ and of $\langle \tilde{\Lambda}_m - \hat{\Lambda}, \hat{\varphi} - \hat{\varphi}_m \rangle_{-1,1}$.

Lemma 1 (Upper bound of Galerkin functional). *The Galerkin functional defined in (18) satisfies*

$$\|\mathcal{G}_m\|_{*,\epsilon} \lesssim \left(\sum_{k=1}^3 (\eta_k^\varphi)^2 \right)^{\frac{1}{2}}.$$

We will give the proof of Lemma 1 with the help of Lemma 2. We use the same ideas as in [29] but due to the different problem, discretization, and error measure some adaptations and comments are required.

Further, we make use of $h_p \approx h_\epsilon \approx h_s$ with $h_s = \text{diam}(\omega_s)$; which follows from the assumed shape regularity.

Lemma 2 (L^2 -approximation with respect to energy norm (9)). *Let $c_p(\psi) = \frac{\int_{\tilde{\omega}_p} \psi \phi_p}{\int_{\tilde{\omega}_p} \phi_p}$ with $\tilde{\omega}_p \subset \omega_p$ the patch around p with respect to a three times uniformly red-refined mesh. Then the L^2 -approximation properties with respect to*

the energy norm (9) hold

$$\|(\psi - c_p(\psi))\phi_p\|_{\omega_p} \lesssim \min\left\{\frac{h_p}{\sqrt{G_c\epsilon}}, \alpha_p^{-\frac{1}{2}}\right\} \|\psi\|_{\epsilon, \omega_p} \quad (23)$$

$$\|(\psi - c_p(\psi))\phi_p\|_{\mathfrak{s}} \lesssim \min\left\{\frac{h_p}{\sqrt{G_c\epsilon}}, \alpha_p^{-\frac{1}{2}}\right\}^{\frac{1}{2}} (G_c\epsilon)^{-\frac{1}{4}} \|\psi\|_{\epsilon, \omega_s}. \quad (24)$$

Proof. As in [29, Lemma 3], we can derive

$$\|\psi - c_p(\psi)\|_{\omega_p} \lesssim h_p \|\nabla\psi\|_{\omega_p} = \frac{h_p}{\sqrt{G_c\epsilon}} \sqrt{G_c\epsilon} \|\nabla\psi\|_{\omega_p}.$$

Using the definition of α_p in (14) it also holds

$$\|\psi - c_p(\psi)\|_{\omega_p} \lesssim \|\psi\|_{\omega_p} \lesssim \alpha_p^{-\frac{1}{2}} \left\| \left(\frac{G_c}{\epsilon} + (1 - \kappa)\boldsymbol{\sigma}(\mathbf{u}_m^n) : \mathbf{E}_{\text{lin}}(\mathbf{u}_m^n) \right)^{\frac{1}{2}} \psi \right\|_{\omega_p}.$$

Together, we deduce the L^2 -approximation property with respect to the energy norm

$$\|\psi - c_p(\psi)\|_{\omega_p} \lesssim \min\left\{\frac{h_p}{\sqrt{G_c\epsilon}}, \alpha_p^{-\frac{1}{2}}\right\} \|\psi\|_{\epsilon, \omega_p}.$$

It remains to derive the L^2 -approximation property for sides \mathfrak{s} . The result [26, Lemma 3.2] can be extended to bilinear finite elements on parallelograms. Thus, we have

$$\|(\psi - c_p(\psi))\phi_p\|_{\mathfrak{s}} \leq \|(\psi - c_p(\psi))\phi_p\|_{0, \omega_s}^{\frac{1}{2}} \|\nabla((\psi - c_p(\psi))\phi_p)\|_{0, \omega_s}^{\frac{1}{2}}$$

We can further proceed as in [29, Lemma 3]. We apply the product rule and triangle inequality

$$\begin{aligned} \|\nabla((\psi - c_p(\psi))\phi_p)\|_{\mathfrak{e}} &\leq \|\nabla(\psi - c_p(\psi))\phi_p\|_{\mathfrak{e}} + \|(\psi - c_p(\psi))\nabla\phi_p\|_{\mathfrak{e}} \\ &\lesssim \|\nabla(\psi - c_p(\psi))\|_{\mathfrak{e}} + h_{\mathfrak{e}}^{-\frac{1}{2}} \|(\psi - c_p(\psi))\|_{\mathfrak{e}}. \end{aligned}$$

Next, we apply the L^2 -approximation property (23) on the elements and $\|\nabla\psi\|_{\omega_s} \leq \frac{1}{\sqrt{G_c\epsilon}} \|\psi\|_{\epsilon, \omega_s}$ to get the L^2 -approximation property on the sides

$$\begin{aligned} &\|(\psi - c_p(\psi))\phi_p\|_{\mathfrak{s}} \\ &\leq \|(\psi - c_p(\psi))\phi_p\|_{0, \omega_s}^{\frac{1}{2}} \|\nabla((\psi - c_p(\psi))\phi_p)\|_{0, \omega_s}^{\frac{1}{2}} \\ &\lesssim h_p^{-\frac{1}{2}} \|(\psi - c_p(\psi))\|_{0, \omega_s} + \|(\psi - c_p(\psi))\phi_p\|_{0, \omega_s}^{\frac{1}{2}} \|\nabla((\psi - c_p(\psi)))\|_{0, \omega_s}^{\frac{1}{2}} \\ &\lesssim h_p^{-\frac{1}{2}} \min\left\{\frac{h_p}{\sqrt{G_c\epsilon}}, \alpha_p^{-\frac{1}{2}}\right\} \|\psi\|_{\epsilon, \omega_s} + \min\left\{\frac{h_p}{\sqrt{G_c\epsilon}}, \alpha_p^{-\frac{1}{2}}\right\}^{\frac{1}{2}} \|\psi\|_{\epsilon, \omega_s}^{\frac{1}{2}} (G_c\epsilon)^{-\frac{1}{4}} \|\psi\|_{\epsilon, \omega_s}^{\frac{1}{2}} \\ &\lesssim \left(\min\left\{\frac{h_p}{\sqrt{G_c\epsilon}}, \alpha_p^{-\frac{1}{2}}\right\}^{\frac{1}{2}} \min\left\{\frac{1}{\sqrt{G_c\epsilon}}, \frac{\alpha_p^{-\frac{1}{2}}}{h_p}\right\}^{\frac{1}{2}} + \min\left\{\frac{h_p}{\sqrt{G_c\epsilon}}, \alpha_p^{-\frac{1}{2}}\right\}^{\frac{1}{2}} (G_c\epsilon)^{-\frac{1}{4}} \right) \|\psi\|_{\epsilon, \omega_s} \\ &\lesssim \min\left\{\frac{h_p}{\sqrt{G_c\epsilon}}, \alpha_p^{-\frac{1}{2}}\right\}^{\frac{1}{2}} (G_c\epsilon)^{-\frac{1}{4}} \|\psi\|_{\epsilon, \omega_s} \end{aligned}$$

□

Together with these preliminary results, we can give the proof of Lemma 1.

Proof of Lemma 1. In order to derive an upper bound of the dual norm of the Galerkin functional, we use the representation (18) and Cauchy-Schwarz inequality

$$\begin{aligned} \langle \mathcal{G}_m, \psi \rangle &\leq \sum_{p \in \mathfrak{N} \setminus \mathfrak{N}^f \setminus \mathfrak{C}} \left(\|G_c \epsilon [\nabla \hat{\varphi}_m]\|_{\gamma_p^I} \|(\psi - c_p(\psi)) \phi_p\|_{\gamma_p^I} \right. \\ &\quad \left. + \|G_c \epsilon \nabla \hat{\varphi}_m \cdot \mathbf{n}_\epsilon\|_{\gamma_p^\Gamma} \|(\psi - c_p(\psi)) \phi_p\|_{\gamma_p^\Gamma} \right. \\ &\quad \left. + \|r(\hat{\varphi}_m)\|_{\omega_p} \|(\psi - c_p(\psi)) \phi_p\|_{\omega_p} \right). \end{aligned} \quad (25)$$

Combining (25), (23), and (24), we get

$$\begin{aligned} \langle \mathcal{G}_m, \psi \rangle_{-1,1} &\lesssim \left(\sum_{p \in \mathfrak{N} \setminus \mathfrak{N}^f \setminus \mathfrak{C}} \left(\min\left\{ \frac{h_p}{\sqrt{G_c \epsilon}}, \alpha_p^{-\frac{1}{2}} \right\}^{\frac{1}{2}} (G_c \epsilon)^{-\frac{1}{4}} \|\epsilon [\nabla \hat{\varphi}_m]\|_{\gamma_p^I} \right. \right. \\ &\quad \left. \left. + \min\left\{ \frac{h_p}{\sqrt{G_c \epsilon}}, \alpha_p^{-\frac{1}{2}} \right\}^{\frac{1}{2}} (G_c \epsilon)^{-\frac{1}{4}} \|\epsilon \nabla \hat{\varphi}_m \cdot \mathbf{n}_\epsilon\|_{\gamma_p^\Gamma} \right. \right. \\ &\quad \left. \left. + \min\left\{ \frac{h_p}{\sqrt{G_c \epsilon}}, \alpha_p^{-\frac{1}{2}} \right\} \|r(\hat{\varphi}_m)\|_{\omega_p} \right)^2 \right)^{\frac{1}{2}} \left(\sum_{p \in \mathfrak{N}} \|\psi\|_{\epsilon, \omega_p}^2 \right)^{\frac{1}{2}} \end{aligned}$$

and thus the bound of the dual norm of the Galerkin functional

$$\|\mathcal{G}_m\|_{*, \epsilon} = \frac{\sup_{\psi \in H^1} \langle \mathcal{G}_m, \psi \rangle_{-1,1}}{\|\psi\|_\epsilon} \lesssim \sum_{k=1}^3 \eta_k^\varphi.$$

□

Lemma 3 (Complementarity residual). *It holds*

$$\left\langle \tilde{\hat{\Lambda}}_m - \hat{\Lambda}, \hat{\varphi} - \hat{\varphi}_m \right\rangle_{-1,1} \lesssim (\eta_4^\varphi)^2.$$

Due to the discretization by bilinear finite elements on parallelograms and linear finite elements on triangles $\mathcal{K}_m^n \subset \mathcal{K}(I_m^n(\varphi_m^{n-1}))$ holds. Thus, for the proof of Lemma 3 we refer to [29, Lemma 4].

Theorem 1 follows from Lemma 1 and Lemma 3.

5 Efficiency of the estimator

This Section provides the proofs of Theorem 2 and 3.

5.1 Local error bound by $\eta_{1,p}^\varphi, \eta_{2,p}^\varphi, \eta_{3,p}^\varphi$

We start with $\eta_{1,p}^\varphi$ for which we use the properties of the element bubble functions $\Psi_\epsilon := c \Pi_{p \in \epsilon} \phi_p$, for triangles and parallelograms, see [28, Chapter 1.3.4]:

- $0 \leq \Psi_\epsilon \leq 1$
- $\|\nabla(\Psi_\epsilon v)\|_\epsilon \lesssim h_\epsilon^{-1} \|v\|_\epsilon$ for all polynomials v

Similar to (14), we define for each element \mathbf{e}

$$\alpha_{\mathbf{e}} := \max_{x \in \mathbf{e}} \left\{ \frac{G_c}{\epsilon} + (1 - \kappa)(\boldsymbol{\sigma}(\mathbf{u}_m^n) : \mathbf{E}_{\text{lin}}(\mathbf{u}_m^n)) \right\} \quad (26)$$

We note that $\frac{G_c}{\epsilon} + (1 - \kappa)(\boldsymbol{\sigma}(\mathbf{u}_m^n) : \mathbf{E}_{\text{lin}}(\mathbf{u}_m^n))|_{\mathbf{e}}$ is constant if \mathbf{e} is a triangle. With respect to the energy norm (9) this implies for all polynomials v

$$\|\Psi_{\mathbf{e}} v\|_{\epsilon, \mathbf{e}} \lesssim (\sqrt{G_c \epsilon} h_{\mathbf{e}}^{-1} + \alpha_{\mathbf{e}}^{\frac{1}{2}}) \|v\|_{\mathbf{e}} \lesssim \max\left\{ \frac{\sqrt{G_c \epsilon}}{h_{\mathbf{e}}}, \alpha_{\mathbf{e}}^{\frac{1}{2}} \right\} \|v\|_{\mathbf{e}}. \quad (27)$$

We recall that for all $p \in \mathfrak{N}$, $\tilde{\omega}_p$ is the patch around p with respect to a three times uniformly red-refined mesh $\tilde{\mathfrak{M}}$ with $\tilde{\mathbf{e}} \in \tilde{\mathfrak{M}}$ and $h_{\tilde{\mathbf{e}}} = ch_{\mathbf{e}}$. We define a linear combination of element bubble functions Ψ_j with respect to all elements $\tilde{\mathbf{e}}_j \subset \mathbf{e}$, i.e., $\theta_{\mathbf{e}} = \sum_{j=1} a_j \Psi_j$. Taking $a_j = 0$ for all elements $\tilde{\mathbf{e}}_j$ containing a node $p \in \mathfrak{N}^{sC}$, we can assert

$$\int_{\tilde{\mathbf{e}}_j} \phi_q \theta_{\mathbf{e}} \phi_p = 0 \quad \forall q \in \mathbf{e}. \quad (28)$$

The other coefficients of the linear combination are chosen such that the bubble function $\theta_{\mathbf{e}}$ fulfills the following conditions

$$\int_{\mathbf{e}} \phi_q \phi_r = \sum_{p \in \mathfrak{N} \setminus \mathfrak{N}^{fC}} \int_{\mathbf{e}} \phi_q \phi_r \theta_{\mathbf{e}} \phi_p \quad \forall q, r \in \mathbf{e} \quad (29)$$

As we have more degrees of freedom (coefficients a_j) than conditions

- three for (28) on a triangle and four for (28) on a parallelogram
- six for (29) on a triangle and ten for (29) on a parallelogram

the construction of a suitable bubble function is possible.

In the following, we make use of the fact that $\bar{r}(\hat{\varphi}_m)$ is a linear finite element function such that (28) implies $c_p(r(\hat{\varphi}_m)\theta_{\mathbf{e}}) = 0$. Further, we exploit (29) and that $\theta_{\mathbf{e}}$ vanishes on the edges. Thus, exploiting (27) for $\theta_{\mathbf{e}}$ instead of $\Psi_{\mathbf{e}}$,

$$\begin{aligned} & \|\bar{r}(\hat{\varphi}_m)\|_{\mathbf{e}}^2 \\ & \lesssim \sum_{p \in \mathfrak{N} \setminus \mathfrak{N}^{fC}} \int_{\mathbf{e}} (\bar{r}(\hat{\varphi}_m))(r(\hat{\varphi}_m)) \theta_{\mathbf{e}} \phi_p + \sum_{p \in \mathfrak{N} \setminus \mathfrak{N}^{fC}} \int_{\mathbf{e}} (\bar{r}(\hat{\varphi}_m) - r(\hat{\varphi}_m)) \bar{r}(\hat{\varphi}_m) \theta_{\mathbf{e}} \phi_p \\ & = \langle \mathcal{G}_m, \bar{r}(\hat{\varphi}_m) \theta_{\mathbf{e}} \rangle - \sum_{p \in \mathfrak{N} \setminus \mathfrak{N}^{fC}} \int_{\gamma_p^I} G_c \epsilon [\nabla \hat{\varphi}_m] \bar{r}(\hat{\varphi}_m) \theta_{\mathbf{e}} \phi_p \\ & \quad + \sum_{p \in \mathfrak{N} \setminus \mathfrak{N}^{fC}} \langle \hat{\Lambda}_m, \phi_p \rangle_{-1,1} c_p(\bar{r}(\hat{\varphi}_m) \theta_{\mathbf{e}}) + \sum_{p \in \mathfrak{N} \setminus \mathfrak{N}^{fC}} \int_{\mathbf{e}} (\bar{r}(\hat{\varphi}_m) - r(\hat{\varphi}_m)) \bar{r}(\hat{\varphi}_m) \theta_{\mathbf{e}} \phi_p \\ & \lesssim \|\mathcal{G}_m\|_{*, \epsilon, \omega_p} \|\bar{r}(\hat{\varphi}_m) \theta_{\mathbf{e}}\|_{\epsilon, \mathbf{e}} + \|\bar{r}(\hat{\varphi}_m) - r(\hat{\varphi}_m)\|_{\mathbf{e}} \|\bar{r}(\hat{\varphi}_m)\|_{\mathbf{e}} \\ & \lesssim \|\mathcal{G}_m\|_{*, \epsilon, \omega_p} \max\left\{ \frac{\sqrt{G_c \epsilon}}{h_{\mathbf{e}}}, \alpha_{\mathbf{e}}^{\frac{1}{2}} \right\} \|\bar{r}(\hat{\varphi}_m)\|_{\mathbf{e}} + \|\bar{r}(\hat{\varphi}_m) - r(\hat{\varphi}_m)\|_{\mathbf{e}} \|\bar{r}(\hat{\varphi}_m)\|_{\mathbf{e}}. \end{aligned}$$

Dividing by $\max\{\frac{\sqrt{G_c\epsilon}}{h_c}, \alpha_c^{\frac{1}{2}}\} \|\tilde{r}(\hat{\varphi}_m)\|_{\mathbf{e}}$ and as $\min\{\frac{h_p}{\sqrt{G_c\epsilon}}, \alpha_c^{-\frac{1}{2}}\} = \left(\max\{\frac{\sqrt{G_c\epsilon}}{h_p}, \alpha_c^{\frac{1}{2}}\}\right)^{-1}$ and $\frac{\alpha_c}{\alpha_p} = C_{\mathbf{e},p} \neq 0$ is a computable constant, we arrive at

$$\eta_{1,p}^\varphi = \min\left\{\frac{h_p}{\sqrt{G_c\epsilon}}, \alpha_p^{-\frac{1}{2}}\right\} \|r(\hat{\varphi}_m)\|_{\omega_p} \lesssim \|\mathcal{G}_m\|_{*,\epsilon,\omega_p} + \text{osc}_p(r) \quad (30)$$

$$\lesssim \|\hat{\varphi} - \hat{\varphi}_m\|_{\epsilon,\omega_p} + \|\hat{\Lambda} - \tilde{\Lambda}_m\|_{*,\epsilon,\omega_p} + \text{osc}_p(r). \quad (31)$$

We note that $C_{\mathbf{e},p} \in [1, 1 + \frac{\max_{x \in \mathbf{e}}(1-\kappa)\sigma(\mathbf{u}_m^x):E_{\text{lin}}(\mathbf{u}_m^x) - \min_{x \in \omega_p}(1-\kappa)\sigma(\mathbf{u}_m^x):E_{\text{lin}}(\mathbf{u}_m^x)}{G_c}]$. In order to prove the lower bound in terms of $\eta_{2,p}^\varphi$, we use the properties of side bubble functions. Following the ansatz given in [26], we define side bubble functions with the help of basis functions belonging to a modified element. On the reference element $\hat{\mathbf{e}}$ the corresponding transformation $\Phi_\delta : \mathbb{R}^2 \rightarrow \mathbb{R}^2$ maps the coordinates x, y to $x, \delta y$ with $\delta \in (0, 1]$. The basis functions on the transformed reference element are given by $\hat{\phi}_{\delta,p} := \hat{\phi}_p \circ \Phi_\delta^{-1}$ on $\Phi_\delta(\hat{\mathbf{e}})$ and $\hat{\phi}_{\delta,p} = 0$ on $\hat{\mathbf{e}} \setminus \Phi_\delta(\hat{\mathbf{e}})$. Let $F_{\mathbf{s}} : \mathbf{e} \rightarrow \hat{\mathbf{e}}$ be the linear transformation which maps \mathbf{s} on $\hat{\mathbf{s}}$ which is the side with the nodes $p_0 = (0, 0)$ and $p_1 = (1, 0)$. The modified side bubble function is defined by $\Psi_{\delta,\mathbf{s}} := \prod_{p \in \hat{\mathbf{s}}} \hat{\phi}_{\delta,p}$. Then it follows from [26, Lemma 3.4] together with the transformation rule

$$\begin{aligned} \|\Psi_{\delta,\mathbf{s}} w\|_{\mathbf{e}} &\lesssim h_c^{\frac{1}{2}} \sqrt{\delta} \|w\|_{\mathbf{s}}, \\ \left\| \frac{\partial}{\partial x_i} (\Psi_{\delta,\mathbf{s}} w) \right\|_{\mathbf{e}} &\lesssim h_c^{-\frac{1}{2}} \sqrt{\delta} \|w\|_{\mathbf{s}}, \quad \forall 1 \leq i \leq n-1 \\ \left\| \frac{\partial}{\partial x_n} (\Psi_{\delta,\mathbf{s}} w) \right\|_{\mathbf{e}} &\lesssim h_c^{-\frac{1}{2}} \frac{1}{\sqrt{\delta}} \|w\|_{\mathbf{s}}. \end{aligned} \quad (32)$$

With respect to the $\|\cdot\|_{\mathbf{e}}$ norm, we get

$$\|\Psi_{\delta,\mathbf{s}} w\|_{\epsilon,\omega_{\mathbf{s}}} \lesssim \left(\sqrt{G_c\epsilon} h_{\mathbf{s}}^{-\frac{1}{2}} \delta^{-\frac{1}{2}} + \alpha_{\mathbf{s}}^{\frac{1}{2}} h_{\mathbf{s}}^{\frac{1}{2}} \delta^{\frac{1}{2}} \right) \|w\|_{\mathbf{s}}. \quad (33)$$

where $\alpha_{\mathbf{s}} := \max_{\tilde{\mathbf{e}} \subset \omega_{\mathbf{s}}} \alpha_{\tilde{\mathbf{e}}}$. Similar to the proof of the lower bound in terms of $\eta_{1,p}^\varphi$, we consider a partition of \mathbf{s} by three uniform refinements. We construct a linear combination $\theta_{\delta,\mathbf{s}} = \sum_j a_j \Psi_{\delta,\tilde{\mathbf{s}}_j}$ of modified side bubble functions $\Psi_{\delta,\tilde{\mathbf{s}}_j}$ with respect to all sides $\tilde{\mathbf{s}}_j$ of the partition of \mathbf{s} such that $c_p([\nabla \hat{\varphi}_m] \theta_{\delta,\mathbf{s}}) = 0$. We choose $a_j = 0$ for all sides $\tilde{\mathbf{s}}_j$ containing a node $p \in \mathfrak{N}^{sC}$ such that for triangles and $p \in \tilde{\mathbf{s}}_j$

$$\int_{\tilde{\mathbf{e}}_j} \theta_{\delta,\mathbf{s}} \phi_p = 0 \quad (34)$$

and for parallelograms and $p \in \tilde{\mathbf{s}}_j$

$$\int_{\tilde{\mathbf{e}}_j} \phi_q \theta_{\delta,\mathbf{s}} \phi_p = 0 \quad \forall q \in \mathbf{e}. \quad (35)$$

The other coefficients of the linear combination are chosen such that the bubble function $\theta_{\delta,\mathbf{s}}$ fulfills the following property for triangles

$$\int_{\mathbf{s}} 1 = \sum_{p \in \mathfrak{N} \setminus \mathfrak{N}^{sC}} \int_{\mathbf{s}} \theta_{\delta,\mathbf{s}} \phi_p \quad (36)$$

and the following property for parallelograms

$$\int_{\mathfrak{s}} \phi_q \phi_r = \sum_{p \in \mathfrak{N} \setminus \mathfrak{N}^{\mathcal{I}^c}} \int_{\mathfrak{s}} \phi_q \phi_r \theta_{\delta, \mathfrak{s}} \phi_p \quad \forall q, r \in \mathfrak{s}. \quad (37)$$

Again, as we have more degrees of freedom (coefficients a_j) than conditions

- one for (34) on a triangle and two for (35) on a parallelogram
- one for (36) on a triangle and three for (37) on a parallelogram

the construction of a suitable bubble function is possible.

We set $w := G_c \epsilon [\nabla \hat{\varphi}_{\mathfrak{m}}]$. Thus, we apply (32), (33). Together with (34), (35) and (36), (37), we get

$$\begin{aligned} \|G_c \epsilon [\nabla \hat{\varphi}_{\mathfrak{m}}]\|_{\mathfrak{s}}^2 &= \sum_{p \in \mathfrak{N} \setminus \mathfrak{N}^{\mathcal{I}^c}} \int_{\mathfrak{s}} G_c^2 \epsilon^2 [\nabla \hat{\varphi}_{\mathfrak{m}}] [\nabla \hat{\varphi}_{\mathfrak{m}}] \theta_{\delta, \mathfrak{s}} \phi_p \\ &\lesssim \langle \mathcal{G}_{\mathfrak{m}}, G_c \epsilon [\nabla \hat{\varphi}_{\mathfrak{m}}] \theta_{\delta, \mathfrak{s}} \rangle + \sum_{p \in \mathfrak{N} \setminus \mathfrak{N}^{\mathcal{I}^c}} \int_{\omega_{\mathfrak{s}}} r(\hat{\varphi}_{\mathfrak{m}}) G_c \epsilon [\nabla \hat{\varphi}_{\mathfrak{m}}] \theta_{\delta, \mathfrak{s}} \phi_p \\ &\quad + \sum_{p \in \mathfrak{N} \setminus \mathfrak{N}^{\mathcal{I}^c}} \left\langle \tilde{\Lambda}_{\mathfrak{m}}, \phi_p \right\rangle_{-1,1} c_p (G_c \epsilon [\nabla \hat{\varphi}_{\mathfrak{m}}] \theta_{\delta, \mathfrak{s}}) \\ &\lesssim \|\mathcal{G}_{\mathfrak{m}}\|_{*, \epsilon, \omega_p} \|G_c \epsilon [\nabla \hat{\varphi}_{\mathfrak{m}}] \theta_{\delta, \mathfrak{s}}\|_{\epsilon, \omega_{\mathfrak{s}}} + \|r(\hat{\varphi}_{\mathfrak{m}})\|_{\omega_{\mathfrak{s}}} \|G_c \epsilon [\nabla \hat{\varphi}_{\mathfrak{m}}] \theta_{\delta, \mathfrak{s}}\|_{\omega_{\mathfrak{s}}} \\ &\lesssim \|\mathcal{G}_{\mathfrak{m}}\|_{*, \epsilon, \omega_p} \left(\sqrt{G_c \epsilon} h_{\mathfrak{s}}^{-\frac{1}{2}} \delta^{-\frac{1}{2}} + \alpha_{\mathfrak{s}}^{\frac{1}{2}} h_{\mathfrak{s}}^{\frac{1}{2}} \delta^{\frac{1}{2}} \right) \|G_c \epsilon [\nabla \hat{\varphi}_{\mathfrak{m}}]\|_{\mathfrak{s}} \\ &\quad + \delta^{\frac{1}{2}} h_{\mathfrak{s}}^{\frac{1}{2}} \|r(\hat{\varphi}_{\mathfrak{m}})\|_{\omega_{\mathfrak{s}}} \|G_c \epsilon [\nabla \hat{\varphi}_{\mathfrak{m}}]\|_{\mathfrak{s}} \end{aligned} \quad (38)$$

Choosing $\delta := \alpha_{\mathfrak{s}}^{-\frac{1}{2}} \min\left\{\frac{\sqrt{G_c \epsilon}}{h_{\mathfrak{s}}}, \alpha_{\mathfrak{s}}^{\frac{1}{2}}\right\} < 1$, we get the first factor

$$\begin{aligned} &\sqrt{G_c \epsilon} h_{\mathfrak{s}}^{-\frac{1}{2}} \alpha_{\mathfrak{s}}^{\frac{1}{4}} \min\left\{\frac{\sqrt{G_c \epsilon}}{h_{\mathfrak{s}}}, \alpha_{\mathfrak{s}}^{\frac{1}{2}}\right\}^{-\frac{1}{2}} + \alpha_{\mathfrak{s}}^{\frac{1}{2}} h_{\mathfrak{s}}^{\frac{1}{2}} \alpha_{\mathfrak{s}}^{-\frac{1}{4}} \min\left\{\frac{\sqrt{G_c \epsilon}}{h_{\mathfrak{s}}}, \alpha_{\mathfrak{s}}^{\frac{1}{2}}\right\}^{\frac{1}{2}} \\ &= (G_c \epsilon)^{\frac{1}{4}} \min\left\{\alpha_{\mathfrak{s}}^{-\frac{1}{2}}, \frac{h_{\mathfrak{s}}}{\sqrt{\epsilon G_c}}\right\}^{-\frac{1}{2}} + \alpha_{\mathfrak{s}}^{\frac{1}{2}} (G_c \epsilon)^{\frac{1}{4}} \min\left\{\alpha_{\mathfrak{s}}^{-\frac{1}{2}}, \frac{h_{\mathfrak{s}}}{\sqrt{\epsilon G_c}}\right\}^{\frac{1}{2}} \\ &\leq (G_c \epsilon)^{\frac{1}{4}} \min\left\{\alpha_{\mathfrak{s}}^{-\frac{1}{2}}, \frac{h_{\mathfrak{s}}}{\sqrt{\epsilon G_c}}\right\}^{-\frac{1}{2}} + (G_c \epsilon)^{\frac{1}{4}} \min\left\{\alpha^{-\frac{1}{2}}, \frac{h_{\mathfrak{s}}}{\sqrt{\epsilon G_c}}\right\}^{-\frac{1}{2}} \underbrace{\alpha_{\mathfrak{s}}^{\frac{1}{2}} \min\left\{\alpha^{-\frac{1}{2}}, \frac{h_{\mathfrak{s}}}{\sqrt{\epsilon G_c}}\right\}}_{\leq 1} \\ &\lesssim (G_c \epsilon)^{\frac{1}{4}} \min\left\{\alpha_{\mathfrak{s}}^{-\frac{1}{2}}, \frac{h_{\mathfrak{s}}}{\sqrt{\epsilon G_c}}\right\}^{-\frac{1}{2}} \end{aligned}$$

and the second factor

$$\begin{aligned} \alpha_{\mathfrak{s}}^{-\frac{1}{4}} \min\left\{\frac{\sqrt{G_c \epsilon}}{h_{\mathfrak{s}}}, \alpha_{\mathfrak{s}}^{\frac{1}{2}}\right\}^{\frac{1}{2}} h_{\mathfrak{s}}^{\frac{1}{2}} &= \min\left\{\frac{h_{\mathfrak{s}}}{\sqrt{G_c \epsilon}}, \alpha_{\mathfrak{s}}^{-\frac{1}{2}}\right\}^{\frac{1}{2}} (\epsilon G_c)^{\frac{1}{4}} \\ &= \min\left\{\frac{h_{\mathfrak{s}}}{\sqrt{G_c \epsilon}}, \alpha_{\mathfrak{s}}^{-\frac{1}{2}}\right\} (\epsilon G_c)^{\frac{1}{4}} \min\left\{\frac{h_{\mathfrak{s}}}{\sqrt{G_c \epsilon}}, \alpha_{\mathfrak{s}}^{-\frac{1}{2}}\right\}^{-\frac{1}{2}} \end{aligned}$$

Thus, dividing (38) by $(G_c \epsilon)^{\frac{1}{4}} \min\left\{\alpha_{\mathfrak{s}}^{-\frac{1}{2}}, \frac{h_{\mathfrak{s}}}{\sqrt{\epsilon G_c}}\right\}^{-\frac{1}{2}} \|G_c \epsilon [\nabla \hat{\varphi}_{\mathfrak{m}}]\|_{\mathfrak{s}}$, we get

$$(G_c \epsilon)^{-\frac{1}{4}} \min\left\{\alpha_{\mathfrak{s}}^{-\frac{1}{2}}, \frac{h_{\mathfrak{s}}}{\sqrt{\epsilon G_c}}\right\}^{\frac{1}{2}} \|G_c \epsilon [\nabla \hat{\varphi}_{\mathfrak{m}}]\|_{\mathfrak{s}} \lesssim \|\mathcal{G}_{\mathfrak{m}}\|_{*, \epsilon, \omega_p} + \min\left\{\frac{h_{\mathfrak{s}}}{\sqrt{G_c \epsilon}}, \alpha_{\mathfrak{s}}^{-\frac{1}{2}}\right\} \|r(\hat{\varphi}_{\mathfrak{m}})\|_{\omega_{\mathfrak{s}}}.$$

Similar to the proof of the lower bound in terms of $\eta_{1,p}^\varphi$, we exploit that $\frac{\alpha_s}{\alpha_p} = C_{s,p} \neq 0$ is a computable constant. Further, we make use of (30) to get the desired lower bound

$$\eta_{2,p}^\varphi \lesssim \|\mathcal{G}_m\|_{*,\epsilon,\omega_p} + \text{osc}_p(r) \lesssim \|\hat{\varphi} - \hat{\varphi}_m\|_{\epsilon,\omega_p} + \|\hat{\Lambda} - \tilde{\Lambda}_m\|_{*,\epsilon,\omega_p} + \text{osc}_p(r). \quad (39)$$

To derive a local lower bound in terms of $\eta_{3,p}^\varphi$, we can proceed in the same way to get

$$\eta_{3,p}^\varphi \lesssim \|\hat{\varphi} - \hat{\varphi}_m\|_{\epsilon,\omega_p} + \|\hat{\Lambda} - \tilde{\Lambda}_m\|_{*,\epsilon,\omega_p} + \text{osc}_p(r). \quad (40)$$

Theorem 2 follows from (31), 39, (40).

5.2 Local error bound in terms of $\eta_{4,p}^\varphi$

In this subsection, we show that also $\eta_{4,p}^\varphi$ constitutes a local lower bound. We proceed almost as in [29]. As the case $\eta_{4,p}^\varphi = 0$ is irrelevant, we can assume $s_p > 0$ which implies that p is a contact node, i.e., $(I_m^n(\varphi_m^{n-1}) - \hat{\varphi}_m)(p) = 0$. Choose a node \hat{q} in ω_p such that $(I_m^n(\varphi_m^{n-1}) - \hat{\varphi}_m)(\hat{q}) \geq (I_m^n(\varphi_m^{n-1}) - \hat{\varphi}_m)(q)$ for all $q \in \omega_p$. We denote the unit vector pointing from p to \hat{q} by $\boldsymbol{\tau}$. We denote the element to which p and \hat{q} belong by $\boldsymbol{\epsilon}_1$ and the element in ω_p which is intersected by $-\boldsymbol{\tau}$, starting in p , is denoted by $\boldsymbol{\epsilon}_N$. The elements between $\boldsymbol{\epsilon}_1$ and $\boldsymbol{\epsilon}_N$ are denoted in order by $\boldsymbol{\epsilon}_i$, $i = 2, \dots, N-1$. For the ease of presentation, we set $v_m := (I_m^n(\varphi_m^{n-1}) - \hat{\varphi}_m)$ in the following. We use Taylor expansion around $v_m(p) = 0$ and the mean value form of the remainder, i.e., there exists a $\zeta_{\boldsymbol{\epsilon}_1}$ such that

$$v_m(\hat{q}) = \underbrace{v_m(p)}_{=0} + \nabla|_{\boldsymbol{\epsilon}_1}(v_m(\zeta_{\boldsymbol{\epsilon}_1})) \cdot (\hat{q} - p). \quad (41)$$

As by definition $v_m(\hat{q}) \geq 0$, it follows that $\nabla|_{\boldsymbol{\epsilon}_1}(v_m(\zeta_{\boldsymbol{\epsilon}_1})) \cdot \boldsymbol{\tau} \geq 0$.

Let $\tilde{q} \in \boldsymbol{\epsilon}_N$ be the point of intersection of $-\boldsymbol{\tau}$ and $\partial\omega_p$. As $v_m(q) \geq 0$ for all $q \in \omega_p$, we can conclude, as in (41), that there exists a $\zeta_{\boldsymbol{\epsilon}_N}$ such that $\nabla|_{\boldsymbol{\epsilon}_N}(v_m(\zeta_{\boldsymbol{\epsilon}_N})) \cdot (-\boldsymbol{\tau}) \geq 0$. Thus, we can add $\nabla|_{\boldsymbol{\epsilon}_N}(v_m(\zeta_{\boldsymbol{\epsilon}_N})) \cdot (-\boldsymbol{\tau})$ to (41)

$$v_m(\hat{q}) \lesssim h_p(\nabla|_{\boldsymbol{\epsilon}_1}(v_m(\zeta_{\boldsymbol{\epsilon}_1})) - \nabla|_{\boldsymbol{\epsilon}_N}(v_m(\zeta_{\boldsymbol{\epsilon}_N}))) \cdot \boldsymbol{\tau} \lesssim h_p|\nabla|_{\boldsymbol{\epsilon}_1}v_m(\zeta_{\boldsymbol{\epsilon}_1}) - \nabla|_{\boldsymbol{\epsilon}_N}v_m(\zeta_{\boldsymbol{\epsilon}_N})|$$

Next, we add and subtract $\nabla|_{\boldsymbol{\epsilon}_i}v_m(\zeta_{\boldsymbol{\epsilon}_i})$ for $i = 2, \dots, N-1$ where the choice of $\zeta_{\boldsymbol{\epsilon}_i} \in \boldsymbol{\epsilon}_i$ for $i \neq \{1, N\}$ is arbitrary and can be set to the midpoint of the elements. We define $\overline{\nabla|_{\boldsymbol{\epsilon}_i}v_m} := \nabla|_{\boldsymbol{\epsilon}_i}v_m(\zeta_{\boldsymbol{\epsilon}_i})$ as a piecewise constant approximation of $\nabla|_{\boldsymbol{\epsilon}_i}v_m$. Thus, we get from the previous inequality

$$v_m(\hat{q}) \lesssim h_p h_p^{-\frac{1}{2}} \|\overline{\nabla(v_m)}\|_{\gamma_p^I}.$$

Further, we exploit

$$\langle \hat{\Lambda}_m, \phi_p \rangle := \int_{\gamma_p^I} G_c \epsilon [\nabla(\hat{\varphi}_m)] \phi_p - \int_{\gamma_p^I} G_c \epsilon \nabla(\hat{\varphi}_m) \phi_p + \int_{\omega_p} r(\hat{\varphi}_m) \phi_p.$$

Putting together and assuming $\frac{h_p}{\sqrt{G_c\epsilon}} \leq \alpha_p^{-\frac{1}{2}}$

$$\begin{aligned}
(\eta_{4,p}^\varphi)^2 &= \langle \hat{\Lambda}_m, \phi_p \rangle c_p (I_m^n(\varphi_m^{n-1}) - \hat{\varphi}_m) \\
&\leq h_p^2 (h_p h_p^{-\frac{1}{2}} \|\overline{\nabla v_m}\|_{\gamma_p^I}) h_p^{-2} \left(\|G_c \epsilon [\nabla \hat{\varphi}_m]\|_{\gamma_p^I} \|\phi_p\|_{\gamma_p^I} + \|G_c \epsilon \nabla \hat{\varphi}_m\|_{\gamma_p^I} \|\phi_p\|_{\gamma_p^I} \right. \\
&\quad \left. + \|r(\hat{\varphi}_m)\|_{\omega_p} \|\phi_p\|_{\omega_p} \right) \\
&\leq (h_p^{\frac{1}{2}} G_c^{-1} \epsilon^{-1} \|G_c \epsilon [\overline{\nabla v_m}]\|_{\gamma_p^I}) \left(\|G_c \epsilon [\nabla \hat{\varphi}_m]\|_{\gamma_p^I} h_p^{\frac{1}{2}} + \|G_c \epsilon \nabla \hat{\varphi}_m\|_{\gamma_p^I} h_p^{\frac{1}{2}} + \|r(\hat{\varphi}_m)\|_{\omega_p} h_p^1 \right) \\
&\leq \left(\frac{h_p^{\frac{1}{2}}}{\sqrt{G_c \epsilon}} \|G_c \epsilon [\overline{\nabla v_m}]\|_{\gamma_p^I} \right) \\
&\quad \left(\|G_c \epsilon [\nabla \hat{\varphi}_m]\|_{\gamma_p^I} \frac{h_p^{\frac{1}{2}}}{\sqrt{G_c \epsilon}} + \|G_c \epsilon \nabla \hat{\varphi}_m\|_{\gamma_p^I} \frac{h_p^{\frac{1}{2}}}{\sqrt{G_c \epsilon}} + \|r(\hat{\varphi}_m)\|_{\omega_p} \frac{h_p}{\sqrt{G_c \epsilon}} \right) \\
&\lesssim \frac{h_p}{G_c \epsilon} \|G_c \epsilon [\nabla \hat{\varphi}_m]\|_{\gamma_p^I}^2 + \frac{h_p}{G_c \epsilon} \|G_c \epsilon \nabla \hat{\varphi}_m\|_{\gamma_p^I}^2 + \frac{h_p^2}{G_c \epsilon} \|r(\hat{\varphi}_m)\|_{\omega_p}^2 + \frac{h_p}{G_c \epsilon} \|G_c \epsilon [\overline{\nabla v_m}]\|_{\gamma_p^I}^2 \\
&\lesssim (\eta_{1,p}^\varphi)^2 + (\eta_{2,p}^\varphi)^2 + (\eta_{3,p}^\varphi)^2 + \frac{h_p}{\sqrt{G_c \epsilon}} \frac{1}{\sqrt{G_c \epsilon}} \|G_c \epsilon [\overline{\nabla v_m}]\|_{\gamma_p^I}^2.
\end{aligned}$$

Thus, together with (31), (39), (40)

$$(\eta_{4,p}^\varphi)^2 \lesssim \|\hat{\varphi} - \hat{\varphi}_m\|_{\epsilon, \omega_p} + \|\hat{\Lambda} - \tilde{\Lambda}_m\|_{*, \epsilon, \omega_p} + \text{osc}_p(r) + \left(\frac{h_p}{\sqrt{G_c \epsilon}} \frac{1}{\sqrt{G_c \epsilon}} \|G_c \epsilon [\overline{\nabla v_m}]\|_{\gamma_p^I}^2 \right)^{\frac{1}{2}}. \quad (42)$$

In the remaining case $\alpha_p^{-\frac{1}{2}} < \frac{h_p}{\sqrt{G_c \epsilon}}$, i.e., in $\eta_{2,p}^\varphi, \eta_{3,p}^\varphi$ it is $\min\{\frac{h_p}{\sqrt{G_c \epsilon}}, \alpha_p^{-\frac{1}{2}}\}^{\frac{1}{2}} (G_c \epsilon)^{-\frac{1}{4}} = \alpha_p^{-\frac{1}{4}} (G_c \epsilon)^{-\frac{1}{4}}$ and in $\eta_{1,p}^\varphi$ it is $\min\{\frac{h_p}{\sqrt{G_c \epsilon}}, \alpha_p^{-\frac{1}{2}}\} = \alpha_p^{-\frac{1}{2}}$. We exploit $h_p \lesssim 1$ and proceed as before

$$\begin{aligned}
(\eta_{4,p}^\varphi)^2 &= \langle \hat{\Lambda}_m, \phi_p \rangle c_p (I_m^n(\varphi_m^{n-1}) - \hat{\varphi}_m) \\
&\leq \left(\frac{h_p^{\frac{1}{2}}}{\sqrt{G_c \epsilon}} \|G_c \epsilon [\overline{\nabla v_m}]\|_{\gamma_p^I} \right) \\
&\quad \left(\|G_c \epsilon [\nabla \hat{\varphi}_m]\|_{\gamma_p^I} \frac{h_p^{\frac{1}{2}}}{\sqrt{G_c \epsilon}} + \|G_c \epsilon \nabla \hat{\varphi}_m\|_{\gamma_p^I} \frac{h_p^{\frac{1}{2}}}{\sqrt{G_c \epsilon}} + \|r(\hat{\varphi}_m)\|_{\omega_p} \frac{h_p}{\sqrt{G_c \epsilon}} \right) \\
&\leq \alpha_p^{-\frac{1}{4}} (G_c \epsilon)^{-\frac{1}{4}} \|G_c \epsilon [\nabla \hat{\varphi}_m]\|_{\gamma_p^I} (\alpha_p^{\frac{1}{4}} G_c^{-\frac{3}{4}} \epsilon^{-\frac{3}{4}} \|G_c \epsilon [\overline{\nabla v_m}]\|_{\gamma_p^I}) \\
&\quad + \alpha_p^{-\frac{1}{4}} (G_c \epsilon)^{-\frac{1}{4}} \|G_c \epsilon \nabla \hat{\varphi}_m\|_{\gamma_p^I} (\alpha_p^{\frac{1}{4}} G_c^{-\frac{3}{4}} \epsilon^{-\frac{3}{4}} \|G_c \epsilon [\overline{\nabla v_m}]\|_{\gamma_p^I}) \\
&\quad + \alpha_p^{-\frac{1}{2}} \|r(\hat{\varphi}_m)\|_{\omega_p} (\alpha_p^{\frac{1}{2}} G_c^{-1} \epsilon^{-1} \|G_c \epsilon [\overline{\nabla v_m}]\|_{\gamma_p^I}) \\
&\lesssim (\eta_{1,p}^\varphi)^2 + (\eta_{2,p}^\varphi)^2 + (\eta_{3,p}^\varphi)^2 + \max\{\alpha_p (G_c \epsilon)^{-2}, \alpha_p^{\frac{1}{2}} (G_c \epsilon)^{-\frac{3}{2}}\} \|G_c \epsilon [\overline{\nabla v_m}]\|_{\gamma_p^I}^2.
\end{aligned}$$

Thus, together with (31), (39), (40), we get

$$\eta_{4,p}^\varphi \lesssim \|\hat{\varphi} - \hat{\varphi}_m\|_{\epsilon, \omega_p} + \|\hat{\Lambda} - \tilde{\Lambda}_m\|_{*, \epsilon, \omega_p} + \text{osc}_p(r) + \max\{\alpha_p (G_c \epsilon)^{-2}, \alpha_p^{\frac{1}{2}} (G_c \epsilon)^{-\frac{3}{2}}\} \|G_c \epsilon [\overline{\nabla v_m}]\|_{\gamma_p^I}^2.$$

This together with (19) and (42) yields Theorem 3.

6 Residual a posteriori estimator for the equation

The residual a posteriori estimator, we give in this section is derived for the solution of the following equation

Problem 7. Let φ_m^{n-1} be given, then find $\hat{\mathbf{u}} \in \mathcal{H}_D^n$ such that

$$\langle g(\varphi_m^{n-1})\boldsymbol{\sigma}(\hat{\mathbf{u}}), \mathbf{E}_{\text{lin}}(\mathbf{w}) \rangle = 0 \quad \forall \mathbf{w} \in \mathcal{H}_0. \quad (43)$$

As discrete approximation of Problem 7, we consider

Problem 8. Let φ_m^{n-1} be given, then find $\hat{\mathbf{u}}_m \in \mathcal{H}_{m,D}^n$ such that

$$\langle g(\varphi_m^{n-1})\boldsymbol{\sigma}(\hat{\mathbf{u}}_m), \mathbf{E}_{\text{lin}}(\mathbf{w}_m) \rangle = 0 \quad \forall \mathbf{w}_m \in \mathcal{H}_{m,0}. \quad (44)$$

We note that the discrete solution $\hat{\mathbf{u}}_m$ of Problem 8 equals the discrete solution \mathbf{u}_m^n of Problem 3 in time step n . Further as φ_m^{n-1} is an approximation of φ^{n-1} , the solution $\hat{\mathbf{u}}$ of Problem 7 is an approximation of \mathbf{u}^n in Problem 1.

Following [27], we derive the residual a posteriori estimator. We define the residual

$$\begin{aligned} \langle \mathcal{R}_m(\hat{\mathbf{u}}_m), \mathbf{w} \rangle_{-1,1} &:= 0 - \langle g(\varphi_m^{n-1})\boldsymbol{\sigma}(\hat{\mathbf{u}}_m), \mathbf{E}_{\text{lin}}(\mathbf{w}) \rangle \\ &= \langle g(\varphi_m^{n-1})\boldsymbol{\sigma}(\hat{\mathbf{u}}), \mathbf{E}_{\text{lin}}(\mathbf{w}) \rangle - \langle g(\varphi_m^{n-1})\boldsymbol{\sigma}(\hat{\mathbf{u}}_m), \mathbf{E}_{\text{lin}}(\mathbf{w}) \rangle. \end{aligned} \quad (45)$$

Let c^* be a constant depending on the largest eigenvalue of Hooke's tensor C and c_* be a constant depending on the smallest eigenvalues of Hooke's tensor. Further, we note that $\kappa \leq g(\varphi_m^{n-1}) \leq 1$. We conclude from (45)

$$\|\mathcal{R}_m(\hat{\mathbf{u}}_m)\|_{-1} = \sup_{\mathbf{w} \in H^1} \frac{\langle g(\varphi_m^{n-1})\boldsymbol{\sigma}(\hat{\mathbf{u}} - \hat{\mathbf{u}}_m), \mathbf{E}_{\text{lin}}(\mathbf{w}) \rangle}{\|\mathbf{w}\|_1} \leq c^* \|\hat{\mathbf{u}} - \hat{\mathbf{u}}_m\|_1 \quad (46)$$

and

$$\|\mathcal{R}_m(\hat{\mathbf{u}}_m)\|_{-1} \geq \frac{\langle g(\varphi_m^{n-1})\boldsymbol{\sigma}(\hat{\mathbf{u}} - \hat{\mathbf{u}}_m), \mathbf{E}_{\text{lin}}(\hat{\mathbf{u}} - \hat{\mathbf{u}}_m) \rangle}{\|\hat{\mathbf{u}} - \hat{\mathbf{u}}_m\|_1} \geq \kappa c_* \|\hat{\mathbf{u}} - \hat{\mathbf{u}}_m\|_1$$

In order to derive the upper bound, we reformulate the residual by means of piecewise integration by parts

$$\begin{aligned} \langle \mathcal{R}_m(\hat{\mathbf{u}}_m), \mathbf{w} \rangle_{-1,1} &= - \int_{\Omega} g(\varphi_m^{n-1})\boldsymbol{\sigma}(\hat{\mathbf{u}}_m) : \mathbf{E}_{\text{lin}}(\mathbf{w}) \\ &= \sum_{\mathbf{e} \in \mathfrak{M}} \int_{\mathbf{e}} \text{div}(g(\varphi_m^{n-1})\boldsymbol{\sigma}(\hat{\mathbf{u}}_m)) \cdot \mathbf{w} - \int_{\partial \mathbf{e}} \mathbf{n}_{\mathbf{e}} g(\varphi_m^{n-1})\boldsymbol{\sigma}(\hat{\mathbf{u}}_m) \cdot \mathbf{w} \\ &= \sum_{\mathbf{e} \in \mathfrak{M}} \int_{\mathbf{e}} (\nabla g(\varphi_m^{n-1}) \cdot \boldsymbol{\sigma}(\hat{\mathbf{u}}_m) + \text{div}\boldsymbol{\sigma}(\hat{\mathbf{u}}_m)g(\varphi_m^{n-1})) \cdot \mathbf{w} - \int_{\partial \mathbf{e}} \mathbf{n}_{\mathbf{e}} g(\varphi_m^{n-1})\boldsymbol{\sigma}(\hat{\mathbf{u}}_m) \cdot \mathbf{w}. \end{aligned} \quad (47)$$

We abbreviate the interior residual by $\mathbf{r}(\hat{\mathbf{u}}_m) := \nabla g(\varphi_m^{n-1}) \cdot \boldsymbol{\sigma}(\hat{\mathbf{u}}_m) + \text{div}\boldsymbol{\sigma}(\hat{\mathbf{u}}_m)g(\varphi_m^{n-1})$, the jump terms between two neighboring elements $\mathbf{e}, \tilde{\mathbf{e}}$

$$\mathbf{J}(\hat{\mathbf{u}}_m) := ((g(\varphi_m^{n-1})\boldsymbol{\sigma}(\hat{\mathbf{u}}_m))|_{\mathbf{e}}\mathbf{n}_{\mathbf{e}} - (g(\varphi_m^{n-1})\boldsymbol{\sigma}(\hat{\mathbf{u}}_m))|_{\tilde{\mathbf{e}}}\mathbf{n}_{\tilde{\mathbf{e}}})$$

and the jump terms at the Neumann boundary by $\mathbf{J}^N(\hat{\mathbf{u}}_m) := ((g(\varphi_m^{n-1})\boldsymbol{\sigma}(\hat{\mathbf{u}}_m))|_{\boldsymbol{\epsilon}}\mathbf{n}_{\boldsymbol{\epsilon}})$. In order to define the quasi-interpolation operator, we need to subclassify the boundary nodes in Dirichlet boundary nodes \mathfrak{N}_m^D and Neumann boundary nodes \mathfrak{N}_m^N with respect to the displacements. Thereby the quasi-interpolation operator is $\mathcal{I}_m(\mathbf{v}) := \sum_{p \in \mathfrak{N}_m} c_p(\mathbf{v})\phi_p \in \mathcal{H}_{m,0}$ for all $\mathbf{v} \in \mathcal{H}_0$ with $c_p(v_i) := \frac{\int_{\omega_p} v_i \phi_p}{\int_{\omega_p} \phi_p}$ for $p \in \mathfrak{N}_m^I$ and $c_p(v_i) := 0$ for $p \in \mathfrak{N}_m^D$, see, e.g., [28, Section 3.5.]. Further, we denote $\gamma_p^N := \Gamma^N \cap \omega_p$. We add $\langle \mathcal{R}_m(\hat{\mathbf{u}}_m), \mathcal{I}_m(\mathbf{w}) \rangle_{-1,1} = 0$ to (47), apply Cauchy-Schwarz and the L^2 -approximation property of the quasi-interpolation operator

$$\begin{aligned} \langle \mathcal{R}_m(\hat{\mathbf{u}}_m), \mathbf{w} \rangle_{-1,1} &= \left\langle \mathcal{R}_m(\hat{\mathbf{u}}_m), \sum_{p \in \mathfrak{N}_m} (\mathbf{w} - c_p(\mathbf{w}))\phi_p \right\rangle_{-1,1} \\ &= \sum_{p \in \mathfrak{N}_m} \int_{\omega_p} \mathbf{r}(\hat{\mathbf{u}}_m) \cdot (\mathbf{w} - c_p(\mathbf{w}))\phi_p \\ &\quad - \int_{\gamma_p^N} \mathbf{J}^I(\hat{\mathbf{u}}_m) \cdot (\mathbf{w} - c_p(\mathbf{w}))\phi_p - \int_{\gamma_p^I} \mathbf{J}^N(\hat{\mathbf{u}}_m) \cdot (\mathbf{w} - c_p(\mathbf{w}))\phi_p \\ &\leq \sum_{p \in \mathfrak{N}_m} \|\mathbf{r}(\hat{\mathbf{u}}_m)\|_{\omega_p} h_p \|\mathbf{w}\|_{1,\omega_p} + \|\mathbf{J}^N(\hat{\mathbf{u}}_m)\|_{\gamma_p^N} h_p^{\frac{1}{2}} \|\mathbf{w}\|_{1,\omega_p} + \|\mathbf{J}^I(\hat{\mathbf{u}}_m)\|_{\gamma_p^I} h_p^{\frac{1}{2}} \|\mathbf{w}\|_{1,\omega_p} \\ &\lesssim \left(\sum_{p \in \mathfrak{N}_m} \|\mathbf{r}(\hat{\mathbf{u}}_m)\|_{\omega_p}^2 h_p^2 + \|\mathbf{J}^I(\hat{\mathbf{u}}_m)\|_{\gamma_p^I}^2 h_p + \|\mathbf{J}^N(\hat{\mathbf{u}}_m)\|_{\gamma_p^N}^2 h_p \right)^{\frac{1}{2}} \left(\sum_{p \in \mathfrak{N}_m} \|\mathbf{w}\|_{1,\omega_p}^2 \right)^{\frac{1}{2}} \end{aligned}$$

Thus, we get the upper bound

$$\|\hat{\mathbf{u}} - \hat{\mathbf{u}}_m\|_1 \lesssim \|\mathcal{R}_m(\hat{\mathbf{u}}_m)\|_{-1} \lesssim \left(\sum_{p \in \mathfrak{N}_m} (\eta_{1,p}^u)^2 + (\eta_{2,p}^u)^2 + (\eta_{3,p}^u)^2 \right)^{\frac{1}{2}}$$

for the error estimator contributions

$$\eta_{1,p}^u := h_p \|\mathbf{r}(\hat{\mathbf{u}}_m)\|_{\omega_p} \quad \eta_{2,p}^u := h_p^{\frac{1}{2}} \|\mathbf{J}^I(\hat{\mathbf{u}}_m)\|_{\gamma_p^I} \quad \eta_{3,p}^u := h_p^{\frac{1}{2}} \|\mathbf{J}^N(\hat{\mathbf{u}}_m)\|_{\gamma_p^N}.$$

In order to prove the lower bound, we use the bubble functions on elements $\Psi_{\boldsymbol{\epsilon}} := \Pi_{p \in \boldsymbol{\epsilon}} \phi_p$ and on sides $\Psi_{\boldsymbol{s}} := \Pi_{p \in \boldsymbol{s}} \phi_p$ with the properties

$$\begin{aligned} \|\rho\|_{\boldsymbol{\epsilon}}^2 &\lesssim \int_{\boldsymbol{\epsilon}} \Psi_{\boldsymbol{\epsilon}} \rho^2 \lesssim \|\rho\|_{\boldsymbol{\epsilon}}^2, & \|\Psi_{\boldsymbol{\epsilon}} \rho\|_{1,\boldsymbol{\epsilon}} &\lesssim h_{\boldsymbol{\epsilon}}^{-1} \|\rho\|_{\boldsymbol{\epsilon}} \\ \|\rho\|_{\boldsymbol{s}}^2 &\lesssim \int_{\boldsymbol{s}} \Psi_{\boldsymbol{s}} \rho^2 \lesssim \|\rho\|_{\boldsymbol{s}}^2, & \|\Psi_{\boldsymbol{s}} \rho\|_{1,\omega_{\boldsymbol{s}}} &\lesssim h_{\boldsymbol{s}}^{-\frac{1}{2}} \|\rho\|_{\boldsymbol{s}} \\ \|\Psi_{\boldsymbol{s}} \rho\|_{\omega_{\boldsymbol{s}}} &\lesssim h_{\boldsymbol{s}}^{\frac{1}{2}} \|\rho\|_{\boldsymbol{s}}. \end{aligned}$$

for all polynomials ρ defined on $\boldsymbol{\epsilon}$ and \boldsymbol{s} . Thus, we get

$$\begin{aligned} \|\mathbf{r}(\hat{\mathbf{u}}_m)\|_{\boldsymbol{\epsilon}}^2 &\lesssim \int_{\boldsymbol{\epsilon}} \mathbf{r}(\hat{\mathbf{u}}_m) \mathbf{r}(\hat{\mathbf{u}}_m) \Psi_{\boldsymbol{\epsilon}} \\ &= \langle \mathcal{R}_m(\hat{\mathbf{u}}_m), \mathbf{r}(\hat{\mathbf{u}}_m) \Psi_{\boldsymbol{\epsilon}} \rangle_{-1,1} \\ &\leq \|\mathcal{R}_m(\hat{\mathbf{u}}_m)\|_{-1,\boldsymbol{\epsilon}} \|\mathbf{r}(\hat{\mathbf{u}}_m) \Psi_{\boldsymbol{\epsilon}}\|_1 \\ &\lesssim \|\mathcal{R}_m(\hat{\mathbf{u}}_m)\|_{-1,\boldsymbol{\epsilon}} h_{\boldsymbol{\epsilon}}^{-1} \|\mathbf{r}(\hat{\mathbf{u}}_m)\|_{\boldsymbol{\epsilon}}. \end{aligned}$$

Dividing by $h_\epsilon^{-1} \|\mathbf{r}(\hat{\mathbf{u}}_m)\|_\epsilon$ and exploiting (46) we arrive at

$$\|\mathbf{r}(\hat{\mathbf{u}}_m)\| \lesssim c^* \|\hat{\mathbf{u}} - \hat{\mathbf{u}}_m\|_{1,\epsilon}.$$

Further, we have

$$\begin{aligned} \|\mathbf{J}^I(\hat{\mathbf{u}}_m)\|_s^2 &\lesssim \int_s \mathbf{J}^I(\hat{\mathbf{u}}_m) \mathbf{J}^I(\hat{\mathbf{u}}_m) \Psi_s \\ &= \left\langle \mathcal{R}_m(\hat{\mathbf{u}}_m), \mathbf{J}^I(\hat{\mathbf{u}}_m) \Psi_s \right\rangle_{-1,1} - \int_{\omega_s} \mathbf{r}(\hat{\mathbf{u}}_m) \mathbf{J}^I(\hat{\mathbf{u}}_m) \Psi_s \\ &\leq \|\mathcal{R}_m(\hat{\mathbf{u}}_m)\|_{-1,\omega_s} \|\mathbf{J}^I(\hat{\mathbf{u}}_m) \Psi_s\|_1 + \|\mathbf{r}(\hat{\mathbf{u}}_m)\|_{\omega_s} \|\mathbf{J}^I(\hat{\mathbf{u}}_m) \Psi_s\|_{\omega_s} \\ &\lesssim \|\mathcal{R}_m(\hat{\mathbf{u}}_m)\|_{-1,\omega_s} h_s^{-\frac{1}{2}} \|\mathbf{J}^I(\hat{\mathbf{u}}_m)\|_s + \|\mathbf{r}(\hat{\mathbf{u}}_m)\|_{\omega_s} h_s^{\frac{1}{2}} \|\mathbf{J}^I(\hat{\mathbf{u}}_m) \Psi_s\|_s. \end{aligned}$$

Dividing by $h_s^{\frac{1}{2}} \|\mathbf{J}^I(\hat{\mathbf{u}}_m) \Psi_s\|_s$ and exploiting (46) we arrive at

$$\|\mathbf{J}^I(\hat{\mathbf{u}}_m)\|_s \lesssim c^* \|\hat{\mathbf{u}} - \hat{\mathbf{u}}_m\|_{1,\omega_s}.$$

The proof for the jump terms at the Neumann boundary follows in the same way. Thus, we get the local lower bounds

$$\eta_{1,p}^u \lesssim \|\hat{\mathbf{u}} - \hat{\mathbf{u}}_m\|_{1,\omega_p}, \quad \eta_{2,p}^u \lesssim \|\hat{\mathbf{u}} - \hat{\mathbf{u}}_m\|_{1,\omega_p}, \quad \eta_{3,p}^u \lesssim \|\hat{\mathbf{u}} - \hat{\mathbf{u}}_m\|_{1,\omega_p}.$$

We note that the constants in the relation of error and upper and lower bounds depend on Hooke's tensor as well as on κ .

7 Numerical results

In this section, we demonstrate the properties of the estimators. We show the adaptively refined grids as well as the convergence and the efficiency index. Therefor, we consider different examples for which we first describe the configurations of the tests.

A single edge notched tension test

We adapt the data from [20]. The domain is a unit square of length 1 mm with a slit on the line $y = 0.5$ mm and $x = [0.25$ mm; 1.0 mm]. The uniform starting mesh consists of squares with a diameter of $h \approx 0.044$ mm. The time step size is $\tau = 10^{-5}$ s. The Lamé coefficients are $\mu = 80.77$ kN mm $^{-2}$ and $\lambda = 121.15$ kN mm $^{-2}$. Further, we have the parameters $G_c = 2.7 \times 10^{-3}$ kN mm $^{-1}$ and $\kappa = 10^{-8}$. We choose $\epsilon \in [0.022; 0.325]$.

At the boundary of the unit square we impose Dirichlet and Neumann boundary conditions. On the upper boundary we pull with Dirichlet values $(u_D)_y = 2 \cdot \tau$ in y -direction, while it is fixed in x -direction, i.e., $(u_D)_x = 0$. At the lower boundary we fix the body in x - and y -direction, i.e., $\mathbf{u}_D = \mathbf{0}$. On the remaining boundaries we have Neumann boundaries with zero values.

A single edge notched shear test

We adapt the data from [20]. The domain is a unit square of length 1 mm with a slit on the line $y = 0.5$ mm and $x = [0.5$ mm; 1.0 mm]. The uniform starting mesh consists of squares with a diameter of $h \approx 0.044$ mm. The time step size is $\tau = 10^{-4}$ s. The Lamé coefficients are $\mu = 80.77$ kN mm $^{-2}$ and $\lambda = 121.15$ kN mm $^{-2}$. Further, we have the parameters $G_c = 2.7 \times 10^{-3}$ kN mm $^{-1}$ and $\kappa = 10^{-8}$. We choose $\epsilon \in [0.022; 0.325]$.

At the boundary of the unit square we impose Dirichlet and Neumann boundary conditions. In x -direction we pull to the left on the upper boundary, i.e., $(u_D)_x = -\tau$ and on the lower boundary we fix the body with $(u_D)_x = 0$. On the remaining boundaries we have zero Neumann values in x -direction. In y -direction we impose zero Dirichlet values everywhere.

An L-shape panel test

We adapt the data from [34]. The L-shaped domain is given by $(0 \text{ mm}, 250 \text{ mm}) \times (0 \text{ mm}, 500 \text{ mm}) \cup [250 \text{ mm}, 500 \text{ mm}) \times (250 \text{ mm}, 500 \text{ mm})$. The uniform starting mesh consists of squares with a diameter of $h \approx 17.67 \text{ mm}$. The time step size is $\tau = 10^{-3} \text{ s}$. The Lamé coefficients are $\mu = 10.95 \text{ kN mm}^{-2}$ and $\lambda = 6.16 \text{ kN mm}^{-2}$. Further, we have the parameters $G_c = 8.9 \times 10^{-5} \text{ kN mm}^{-1}$ and $\kappa = 10^{-8}$.

At the bottom boundary we fix the body with Dirichlet boundary conditions $\mathbf{u}_D = \mathbf{0}$. Further, at the small horizontal boundary line at the right where $y = 250 \text{ mm}$ and $x = [470 \text{ mm}; 500 \text{ mm}]$ we push with Dirichlet boundary conditions in y -direction, i.e., $(u_D)_y = \tau$. At all other boundaries and directions we have zero Neumann values.

Remark 4. *The physics of the single edge notched shear test and the L-shape panel test demand to use the stress splitting as in Problem 2 and 4. The stress splitting enters in the derivation of the estimator η^φ but not in the estimator η^u which has been derived as standard residual estimator for an elliptic problem.*

For the solution a complementarity formulation of the variational inequality as described in [19, Section 4] is used. The calculations are performed using [13] based on the finite element library [2].

7.1 Adaptive refinement using the estimator η^φ

7.1.1 Adaptively refined grids

We show the adaptively refined grids steered by the estimator η^φ and the corresponding phase field. For the tension and the shear test, we show grids and the phase field at two different time steps. One time step is chosen in the middle of the simulation when the crack already started to grow and the second time step is the moment when the crack reaches the boundary. We see for the tension test in Figure 1, for the shear test in Figure 2, and for the L-shape panel test in Figure 3 that the crack path is well resolved.

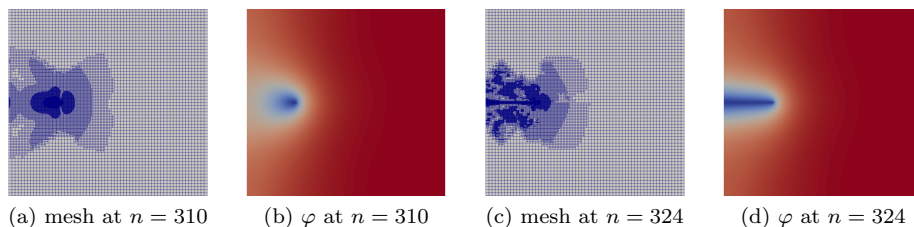


Figure 1: Tension test with $\epsilon = 0.088$ at different time points after six adaptive refinement steps based on the estimator η^φ . Values of $\varphi \approx 1$ are colored in red, values $\varphi \approx 0$ are blue.

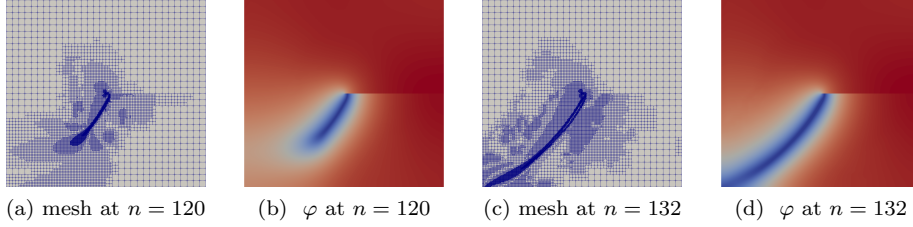


Figure 2: Shear test with $\epsilon = 0.088$ at different time points after five adaptive refinement steps based on the estimator η^φ . Values of $\varphi \approx 1$ are colored in red, values $\varphi \approx 0$ are blue.

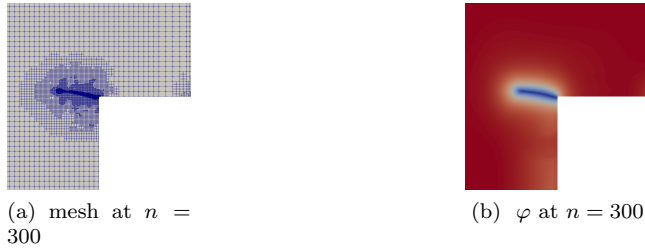


Figure 3: L-shape test with $\epsilon = 20$ at different time points after five adaptive refinement steps based on the estimator η^φ . Values of $\varphi \approx 1$ are colored in red, values $\varphi \approx 0$ are blue.

7.1.2 Crack and bulk energy and load-displacement curves

Further, we show the crack and the bulk energy as well as plots for the load-displacement curves for all three tests in Figures 4, 5 and 6. The curves converge with the adaptive refinement.

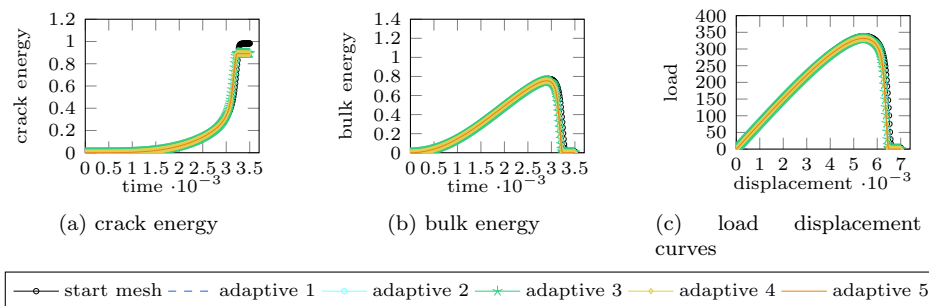
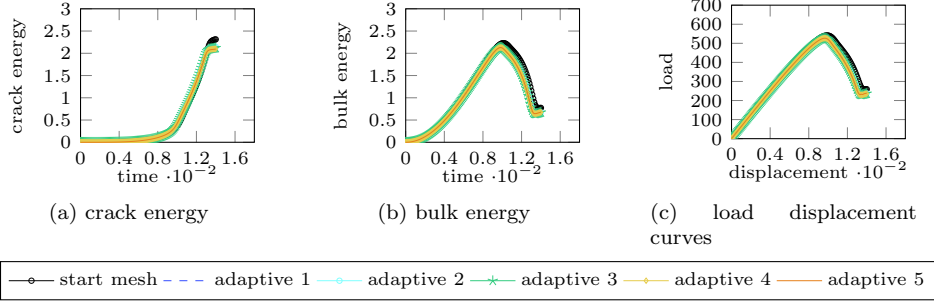
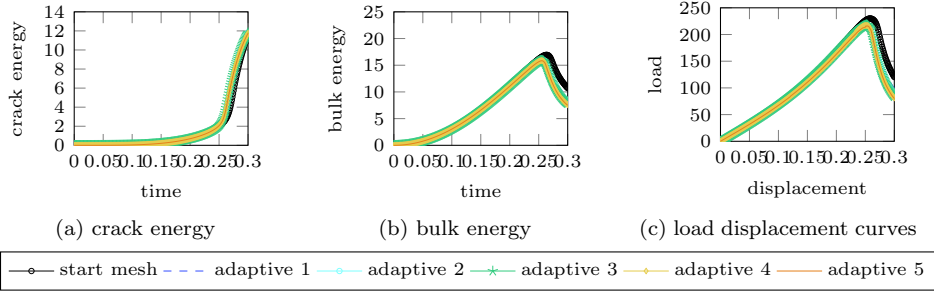


Figure 4: Tension test with $\epsilon = 0.088$.

Figure 5: Shear test with $\epsilon = 0.088$.Figure 6: L-shape test with $\epsilon = 20$.

7.1.3 Convergence in different error norms

To demonstrate the convergence behavior of the errors, we compute reference solutions $\underline{\mathbf{u}}^n$, $\underline{\varphi}^n$ on a finer mesh which has been at least three times more uniformly refinement than the adaptive meshes on which the solutions \mathbf{u}_m^n and φ_m^n have been computed.

To measure the errors in φ and \mathbf{u} , we use the energy norm in φ given by

$$\|\underline{\varphi}^n - \varphi_m^n\|_{\epsilon}^2 = G_c \epsilon \|\nabla(\underline{\varphi}^n - \varphi_m^n)\|^2 + \left(\frac{G_c}{\epsilon} + (1 - \kappa) \boldsymbol{\sigma}(\underline{\mathbf{u}}^n) : \mathbf{E}_{\text{lin}}(\underline{\mathbf{u}}^n) \right)^{\frac{1}{2}} (\underline{\varphi}^n - \varphi_m^n)^2$$

and the energy norm in \mathbf{u} given by

$$\|\underline{\mathbf{u}}^n - \mathbf{u}_m^n\|_{Eu}^2 := \int_{\Omega} g(\varphi_m^n) \boldsymbol{\sigma}(\underline{\mathbf{u}}^n - \mathbf{u}_m^n) : \mathbf{E}_{\text{lin}}(\underline{\mathbf{u}}^n - \mathbf{u}_m^n)$$

As expected the adaptive refinement gives rise to a stronger error reduction for the error in φ than the uniform refinement. But this does not only hold for the error in φ but also for the error in \mathbf{u} although the adaptive refinement has been

steered by the estimator η^φ .



Figure 7: Convergence in different error measures for tension test at $n = 280$ with $\epsilon = 0.088$ and adaptive refinement based on the estimator η^φ . Left: energy norm in φ , Right: energy norm in u .



Figure 8: Convergence in different error measures for shear test at $n = 107$ with $\epsilon = 0.088$ and adaptive refinement based on the estimator η^φ . Left: energy norm in φ , Right: energy norm in u .



Figure 9: Convergence in different error measures for L-shape test at $n = 200$ with $\epsilon = 20$ and adaptive refinement based on the estimator η^φ . Left: energy norm in φ , Right: energy norm in u .

7.1.4 Efficiency index

In this subsection, we visualize the efficiency index, i.e., the quotient of η^φ and the energy norm $\|\varphi^n - \varphi_m^n\|_\epsilon$. We compare it to the efficiency index for a non-robust residual estimator which can be easily derived without taking care of the aspect of robustness. For this we derived a residual-type a posteriori estimator for Problem 5 with respect to the H^1 -norm of the error, not paying attention to the ϵ -dependency. The derivation basically follows along the lines of Section 4 and 5. The proofs would be simplified as the standard versions of the L^2 -approximation and the bubble functions can be used. Thus, instead of the energy norm the H^1 -norm is taken whenever calculating efficiencies for the

non-robust estimator.

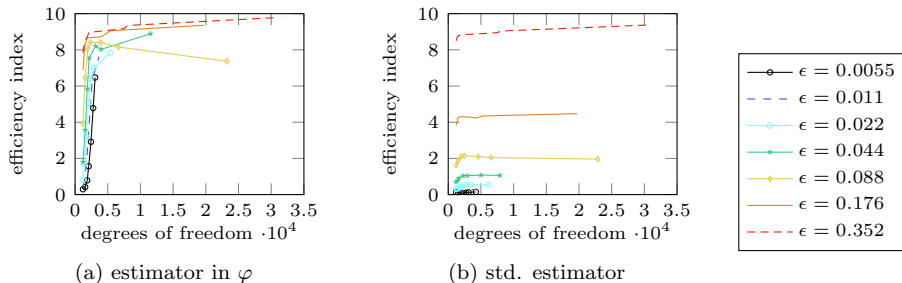


Figure 10: Efficiency index for tension test in time step $n = 280$ with estimator η^φ and standard estimator on different meshes

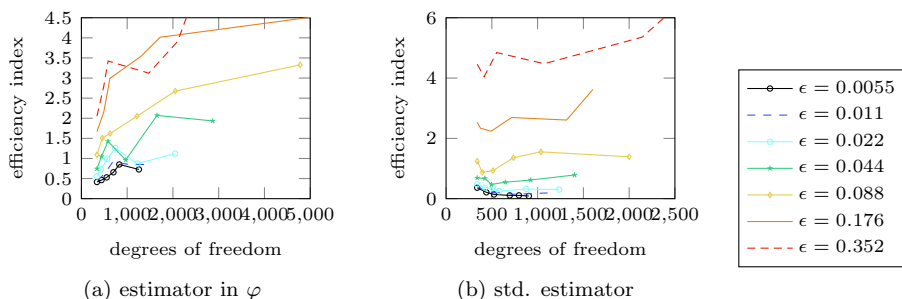


Figure 11: Efficiency index for shear test in time step $n = 107$ with estimator η^φ and standard estimator on different meshes

As is clearly visible in Figures 10 and 11, the efficiency indices for the new estimator are robust with respect to the variation of ϵ while the efficiency tends to zero for the standard estimator.

7.2 Adaptive refinement using both estimators η^u and η^φ

In this subsection, we investigate the adaptive refinement which is steered by both estimators, the estimator η^φ from Section 3 and η^u from Section 6. In the implementation, we normalize both estimators and add them before the marking strategy is called. In the following we solely show numerical results for the tension and the shear tests because the L-shape test is modeled by inhomogeneous Dirichlet boundary conditions on a small portion of the boundary. The estimator η^u correctly identifies the singularity induced by this boundary condition and resolves the resulting singularity. This is reasonable for the discretization error but contains a model error as the Dirichlet conditions imitate that the area is vertically clamped, see [34].

7.2.1 Adaptively refined grids

Comparing Figures 12 and 13 with the Figures 1 and 2, we see that the adaptive refinement is different. While for the tension test in Figure 12 the crack path is still well resolved, the influence of the estimator η^u is stronger for the shear

test and leads to a strong refinement of the origin of the crack and thus to less refinement of the crack path.

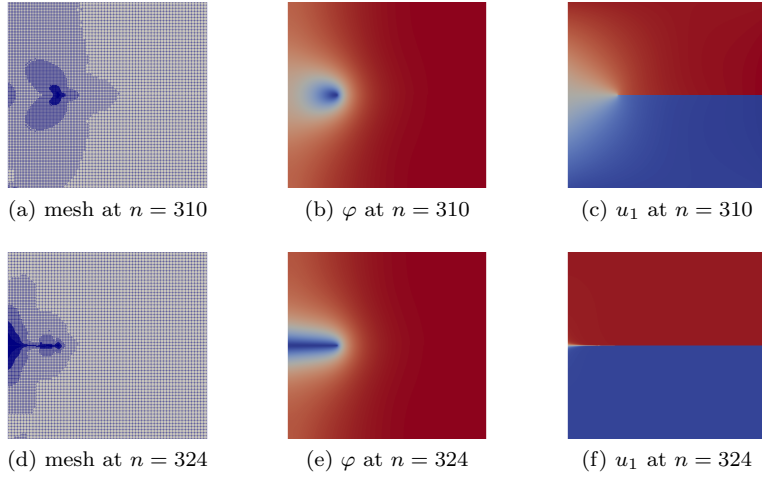


Figure 12: Tension test with $\epsilon = 0.088$ at different time points after six adaptive refinement steps based on the estimators η^φ and η^u . Values of $\varphi \approx 1$ and $u_1 \gg 0$ are colored in red, values $\varphi \approx 0$ and $u_1 \ll 0$ are blue.

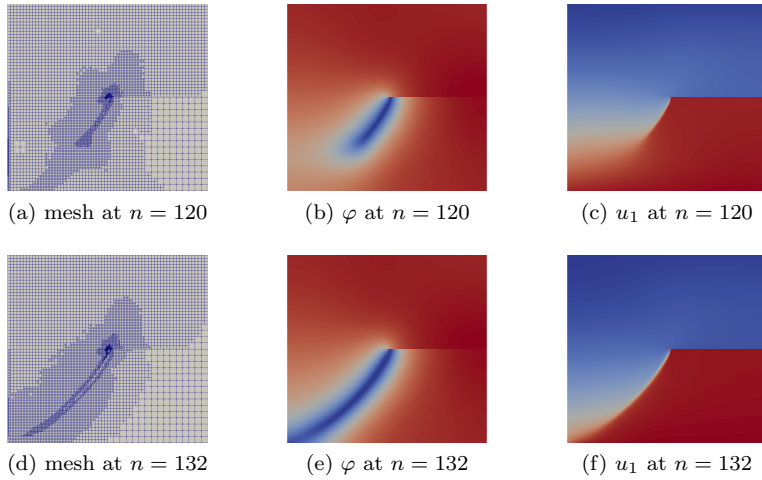


Figure 13: Shear test with $\epsilon = 0.088$ at different time points after six adaptive refinement steps based on the estimators η^φ and η^u . Values of $\varphi \approx 1$ and $u_1 \gg 0$ are colored in red, values $\varphi \approx 0$ and $u_1 \ll 0$ are blue.

7.2.2 Convergence in different error norms

Finally, we show the convergence behavior for the tension and shear test using adaptive refinement steered by both estimators η^φ and η^u compared to uniform refinement. Especially for the shear test it is obvious that the influence of the

estimator η^u improve the convergence order for the error in \mathbf{u} .



Figure 14: Convergence in different error measures for tension test at $n = 280$ with $\epsilon = 0.088$ and adaptive refinement based on the estimators η^φ and η^u . Left: energy norm in φ , Right: energy norm in u .



Figure 15: Convergence in different error measures for shear test at $n = 107$ with $\epsilon = 0.088$ and adaptive refinement based on the estimators η^φ and η^u . Left: energy norm in φ , Right: energy norm in u .

Acknowledgments. This work was funded by the Deutsche Forschungsgemeinschaft (DFG, German Research Foundation) – Projektnummer 392587580 – SPP 1748

References

- [1] M. Ambati, T. Gerasimov, and L. De Lorenzis. Phase-field modeling of ductile fracture. *Comput. Mech.*, pages 1–24, 2015.
- [2] D. Arndt, W. Bangerth, D. Davydov, T. Heister, L. Heltai, M. Kronbichler, M. Maier, J.-P. Pelteret, B. Turcksin, and D. Wells. The deal.II finite element library: Design, features, and insights. *Comput. Math. Appl.*, 81:407–422, 2021.
- [3] M. Artina, M. Fornasier, S. Micheletti, and S. Perotto. Anisotropic mesh adaptation for crack detection in brittle materials. *SIAM J. Sci. Comput.*, 37(4):B633–B659, 2015.
- [4] S. Bartels and C. Carstensen. Averaging techniques yield reliable a posteriori finite element error control for obstacle problems. *Numer. Math.*, 99(2):225–249, 2004.
- [5] M. J. Borden, T. J. Hughes, C. M. Landis, and C. V. Verhoosel. A higher-order phase-field model for brittle fracture: Formulation and analysis within the isogeometric analysis framework. *Comput. Methods Appl. Mech. Engrg.*, 273:100–118, 2014.
- [6] M. J. Borden, C. V. Verhoosel, M. A. Scott, T. J. R. Hughes, and C. M. Landis. A phase-field description of dynamic brittle fracture. *Comput. Methods Appl. Mech. Engrg.*, 217:77–95, 2012.
- [7] B. Bourdin, G. A. Francfort, and J.-J. Marigo. The variational approach to fracture. *J. Elasticity*, 91(1–3):1–148, 2008.

- [8] S. Burke, C. Ortner, and E. Süli. An adaptive finite element approximation of a variational model of brittle fracture. *SIAM J. Numer. Anal.*, 48(3):980–1012, 2010.
- [9] S. Burke, C. Ortner, and E. Süli. An adaptive finite element approximation of a generalized Ambrosio-Tortorelli functional. *M3AS*, 23(9):1663–1697, 2013.
- [10] Z. Chen and R. Nochetto. Residual type a posteriori error estimates for elliptic obstacle problems. *Numer. Math.*, 84(4):527–548, 2000.
- [11] F. Fierro and A. Veeseer. A posteriori error estimators for regularized total variation of characteristic functions. *SIAM J. Numer. Anal.*, 41(6):2032–2055, 2003.
- [12] G. Francfort and J.-J. Marigo. Revisiting brittle fracture as an energy minimization problem. *J. Mech. Phys. Solids*, 46(8):1319–1342, 1998.
- [13] C. Goll, T. Wick, and W. Wollner. DOpElib: Differential equations and Optimization Environment; A goal oriented software library for solving PDEs and optimization problems with PDEs. *Archive of Numerical Software*, 5(2):1–14, 2017.
- [14] A. Griffith. The phenomena of rupture and flow in solids. *Philos. Trans. R. Soc. Lond.*, 221:163–198, 1921.
- [15] T. Gudi and K. Porwal. A posteriori error control of discontinuous Galerkin methods for elliptic obstacle problems. *Math. Comp.*, 83(286):579–602, 2014.
- [16] T. Gudi and K. Porwal. A posteriori error estimates of discontinuous Galerkin methods for the Signorini problem. *J. Comput. Appl. Math.*, 292:257–278, 2016.
- [17] T. Heister, M. F. Wheeler, and T. Wick. A primal-dual active set method and predictor-corrector mesh adaptivity for computing fracture propagation using a phase-field approach. *Comput. Methods Appl. Mech. Engrg.*, 290:466–495, 2015.
- [18] R. Krause, A. Veeseer, and M. Walloth. An efficient and reliable residual-type a posteriori error estimator for the Signorini problem. *Numer. Math.*, 130(1):151–197, 2015.
- [19] K. Mang, M. Walloth, T. Wick, and W. Wollner. Mesh adaptivity for quasi-static phase-field fractures based on a residual-type a posteriori error estimator. *GAMM-Mitt.*, 43(1):e202000003, 22, 2020.
- [20] C. Miehe, M. Hofacker, and F. Welschinger. A phase field model for rate-independent crack propagation: robust algorithmic implementation based on operator splits. *Comput. Methods Appl. Mech. Engrg.*, 199(45-48):2765–2778, 2010.
- [21] C. Miehe, F. Welschinger, and M. Hofacker. Thermodynamically consistent phase-field models of fracture: variational principles and multi-field FE implementations. *Internat. J. Numer. Methods Engrg.*, 83(10):1273–1311, 2010.
- [22] K.-S. Moon, R. H. Nochetto, T. von Petersdorff, and C.-S. Zhang. A posteriori error analysis for parabolic variational inequalities. *M2AN Math. Model. Numer. Anal.*, 41(3):485–511, 2007.
- [23] R. H. Nochetto, K. G. Siebert, and A. Veeseer. Fully localized a posteriori error estimators and barrier sets for contact problems. *SIAM J. Numer. Anal.*, 42(5):2118–2135, 2005.
- [24] A. Schlüter, A. Willenbücher, C. Kuhn, and R. Müller. Phase field approximation of dynamic brittle fracture. *Comput. Mech.*, 54(5):1141–1161, 2014.
- [25] A. Veeseer. Efficient and reliable a posteriori error estimators for elliptic obstacle problems. *SIAM J. Numer. Anal.*, 39(1):146–167, 2001.
- [26] R. Verfürth. Robust a posteriori error estimators for a singularly perturbed reaction-diffusion equation. *Numer. Math.*, 78(3):479–493, 1998.

- [27] R. Verfürth. A review of a posteriori error estimation techniques for elasticity problems. *Comput. Methods Appl. Mech. Engrg.*, 176(1-4):419–440, 1999. New advances in computational methods (Cachan, 1997).
- [28] R. Verfürth. *A posteriori error estimation techniques for finite element methods*. Numerical Mathematics and Scientific Computation. Oxford University Press, Oxford, 2013.
- [29] M. Walloth. Residual-type a posteriori estimators for a singularly perturbed reaction-diffusion variational inequality – reliability, efficiency and robustness. Preprint 1812.01957, arXiv, 2018.
- [30] M. Walloth. A reliable, efficient and localized error estimator for a discontinuous Galerkin method for the Signorini problem. *Appl. Numer. Math.*, 135:276–296, 2019.
- [31] M. Walloth. Residual-type a posteriori error estimator for a quasi-static Signorini contact problem. *IMA J. Numer. Anal.*, 40(3):1937–1971, 2020.
- [32] A. Weiss and B. I. Wohlmuth. A posteriori error estimator for obstacle problems. *SIAM J. Sci. Comput.*, 32(5):2627–2658, 2010.
- [33] T. Wick. Goal functional evaluations for phase-field fracture using pu-based dwr mesh adaptivity. *Comput. Mech.*, 57(6):1017–1035, 2016.
- [34] B. Winkler. *Traglastuntersuchungen von unbewehrten und bewehrten Betonstrukturen auf der Grundlage eines objektiven Werkstoffgesetzes für Beton*. PhD thesis, Universität Innsbruck, 2001.
- [35] Q. Zou, A. Veese, R. Kornhuber, and C. Gräser. Hierarchical error estimates for the energy functional in obstacle problems. *Numer. Math.*, 117(4):653–677, 2011.